雑誌

発表者氏名	論文タイトル名	発表誌名	巻号	ページ	出版年
Murata H.. Ihara Y., Nakamura H., Yodoi J., Sumikawa K., and Kondo T.	Glutaredoxin exerts anti-apoptotic effect by regulating redox state of Akt.	J. Brol. Chem.	278	50226-33	2003
Atarashi, R., Nishida, N., Shigematsu, K., Goto, S.. Kondo. T., and Sakaguchi, S.	Deletron of N terminal residues 23-88 from prion protein (PrP) abrogatesthe potential to rescue PrP-like protein/Doppel-induced neurodegeneration.	J. Brol. Chem.	278 (31)	28944-28949	2003
Muroya, T., Ihara. Y.. Ikeda, S , Yasuoka, C., Miyahara, Y., Urata, Y., Kondo, T., and Kohno, S.	Oxidative modulation of NF-κβ Signaling by oxidized low-density lipopretein.	Biochem Brophys. Res. Commun.	309	900-905	2003
Mitsuta, K., Matsuse, H., Fukushima, C., Kawano T., Tomari, S., Obase, Y., Goto, S., Urata, Y., Shimada, T., Kondo, T., and Kohno. S.	Production of TNF-α by peripheral blood mononuclear cells through activation of nuclear factor κB by specific allergen stimulation in patients with atopic asthma.	Allergy Asthlna Proc.	24	19-26	2003
Okuno, S., Sato, H., Kuriyama-Matumura, K., Tamba, M., Sohda, S., Hamada, H., Yoshikawa, H., Kondo, T., and Bannai, S.	Role of cystine transport in intracellular glutathione level and cisplatin resistance in human ovarian cancer cell lines.	British. J. Cancer.	88	951-956	2003
Shimizu, K., Naito, S., Urata, Y., Takamiyagi, A., Bae, S.J., Ogawa, F., Kondo, T., and Katayama, I.	The induction of eme oxygenase-1 by exogenous nitric oxide in ex vivo normal human skin.	J. Dermatol.	30	17-25	2003.
Ohira, A., Tanito, M., Kaidzu, S., Kondo. T.	Glutathione peroxidase induced in rat retinas to counteract photic injury.	Invest. Ophth. Vis. Sci.	44(3)	1230-1236	2003
Ihara, Y.	A novel regulatory mechanism of apoptosis by calreticulin, a molecular chaperonr in the endoplasmic reticulum.	Acta. Med. Nagasaki.	48	85-92	2003

発表者氏名	論文タイトル名	発表誌名	巻号	ページ	出版年
K, Muta., H, Masuzaki., Y, Urata., S, Goto., T, Ishimaru., and T Kondo	Gene expression of nitric oxide synthase and heme oxygenase in placental villi during pregnancy with and without intrauterine growth restriction.	J. Clin. Biochem. Nutr.	32	11-21	2002
Tanimura, S., Nomura, K., Ozaki, K., Thujrmoto, M., Kondo, T., and Kohno, M.	Prolonged Nuclear Retention of Activated Extracellular Signal-Regulated Kinase1/2 is Required for Hepatocyte Growth Factor-induced Cell Motility.	J. Biol. Chem.	277	28256-28264	2002
Nagata, J., KiJima, H., Hatanaka, H., Asai, S., Miyachi, H., Abe, Y., Yamazaki, H., Nakamura, M., Watanabe, N., Mine, T., Kondo, T., Scanlon, K. J., and Ueyama, Y.	Reversal of drug resistance using hammerhead ribozymes against multidrug resistance-associated protein andd multidrug resistance 1 gene.	International J Oncology.	21	1021-1026	2002
Ihara, Y., Manabe, S., Kanda, M., Kawano, H., Nakayama, T., Sekine, I., Kondo, T., and Ito, Y.	Increased expression of protein C-mannosylation in the aortic vessels of diabetic rats.	**Glycobiology**		in press.	2004
Soh, Y., Goto, S., Kitajima, M., Moriyama, S., Kotera, K., Nakayama, T., Nakajima, H., Kondo, T., and Ishimaru, T.	Nuclear Localization of Glutathione S-Transferase π is an Evaluation Factor for Drug Resistance in Gynecological Cancers.	**Clinical Oncology.**		In press.	2004
Yasuoka, C., Ihara, Y., Ikeda, S., Miyahara, Y., Kondo, T., and Kohno, S.	Antiapoptptic activity of Akt is down-regulated by Ca^{2+} in myocardiac H9c2 cell. – Evidence of Ca^{2+}-dependent regulation of protein phosphatase 2Ac.	**J. Biol. Chem.**	279	51182-51192	2004
Kamada,K., Goto, S., Okunaga, T., Ihara, Y., Tsuji, K., Kawai, Y., Uchida, K., Osawa, T., Matsuo, T., Nagata, I., and Kondo, T.	Nuclear glutathione S-transferase prevents apoptosis by reducing the oxidative stress-induced formation of exocyclic DNA adducts.	**Free Radical. Biol. Med.**	37(11)	1875-1884	2004
Tarumoto, T., Nagai, T., Ohmine, K., Miyoshi, T., Nakamura, M., Kondo, T., Mitsugi, K., Muroi, K., Komatsu, N., and Ozawa, K.	Ascorbic acid restores sensitivity to imatinib via suppression of Nrf2-dependent gene expression in the imatinib-resistant cell line.	**Experimental Hematology.**	32	375-381	2004

	論文タイトル名	発表誌名	巻号	ページ	出版年
池田聡司、近藤宇史	フリーラジカルの産生と消去機構	『分子呼吸器病』 (先端医学社)	6:2	20-26	2002
後藤信治、谷政治、鎌田健作、飯田桂子、浦田芳重、井原義人、近藤宇史、奥村寛	抗酸化因子の遺伝子制御と放射線感受性	『広島医学』	55:3	258-260	2002
井原義人、近藤宇史	分子シャペロンとレドックス制御	THE LUNG メディカルレビュー(株)	10(4)	59-63	2002
近藤宇史、後藤信治	[合成系]g-グルタミルシステインシンテターゼ	Vitamins(Japan)	76(11)	515-519	2002
村田寛明、近藤宇史	『急性肺損傷と酸化ストレス』	医学の歩み 【別冊・呼吸器疾患 2003-2005】		14-16	2003

雑誌

発表者氏名	論文タイトル名	発表誌名	巻号	ページ	出版年
Murata H. and Ihara Y., et al.	Glutaredoxin exerts antiapoptotic effect by regulating redox state of Akt.	J. Biol. Chem.	278	50226-50233	2003
Muroya T., and Ihara Y., et al.	Oxidative modulation of NF-kB signaling by oxidized low-density lipoprotein. Biochem. Biophys. Res. Commun	Biochem. Biophys. Res. Commun.	309	905-910	2003
Yasuoka C., Ihara Y., et al.	Antiapoptotic activity of Akt is down-regulated by Ca^{2+} in myocardiac H9c2 cells. Evidence of Ca^{2+}-dependent regulation of protein phosphatase 2Ac.	J. Biol. Chem.	279	51182-51192	2004
Kamada K., Ihara Y., et al.	Nuclear glutathione S-transferase • prevents apoptosis by reducing the oxidative stress-induced formation of exocyclic DNA products.	Free Radic. Biol. Med.	37	1875-1884	2004
Ihara Y., et al .	Increased expression of protein C-mannosylation in the aortic vessels of diabetic Zucker rats.	Glycobiology	in press		2005
Ihara Y., Kageyama K., and Kondo T.	: Overexpression of calreticulin sensitizes SERCA2a to oxidative stress.	Biochem. Biopys. Res. Commun	in press		,2005

雑誌

発表者氏名	論文タイトル名	発表誌名	巻号	ページ	出版年
井上勝美	Pathological analyses of long-term intracoronary Palma-Schatz stenting ; Is its efficacy permanent?	Cardiovascular Pathology		109-115	2004
Sakai K, Nakagawa Y, Kimura T, Ando K, Yokoi H, Iwabuchi M, Inoue K, Nosaka H, Nobuyoshi M.	Primary angioplasty of unprotected left main coronary artery for acute anterolateral myocardial infarction.	JInvasive Cardiol.	Nov;16(11)	621-5	2004
Nishiyama K, Okino S, Andou J, Nakagawa Y, Nobuyoshi M.	Coronary angioplasty reduces free wall rupture and improves mortality and morbidity of acute myocardial infarction.	J Invasive Cardiol.	Oct;16(10)	554-8	2004
Ozaki K, Inoue K, Sato H, Iida A, Ohnishi Y, Sekine A, Sato H, Odashiro K, Nobuyoshi M, Hori M, Nakamura Y, Tanaka T.	Functional variation in LGALS2 confers risk of myocardial infarction and regulates lymphotoxin-alpha secretion in vitro.	Nature	May 6;429(6987)	72-5	2004
Inoue K, Abe K, Ando K, Shirai S, Nishiyama K, Nakanishi M, Yamada T, Sakai K, Nakagawa Y, Hamasaki N, Kimura T, Nobuyoshi M, Miyamoto TA.	Pathological analyses of long-term intracoronary Palmaz-Schatz stenting; Is its efficacy permanent? :	Cardiovasc Pathol	Mar-Apr;13(2	109-15	2004

雑誌

発表者氏名	論文タイトル名	発表誌名	巻号	ページ	出版年
M., Miyamae, H., FuijWara, M., Tanaka, R., Yokota, G., Takemura, S., Itoh, N., Domae, Vincent M Figueredo	OXygen radicals mediate ultrastructura! and metabolic protection of preconditioning in vivo in pig hearts	Exp. Clin. Cardiol.	7(4)	173-179	2003
K., Hayashida, M., Tanaka, H., Morita, F., Hayashi, T., Inada, H., Suzuki, T., Sakamoto, M., Katsuragawa, H., Hibino, H., Kambara.	Chlamydia pneumoniae seropositivity predicts the risk of restenosis after percutaneous transluminal coronary angioplasty.	Heart Vessels	16	137-145	2002

雑誌

発表者氏名	論文タイトル名	発表誌名	巻号	ページ	出版年
H. Yoshioka, N. Hayashi, K. Ueyama, et. al.	Urinary Incontinence in Elderly Patients with Senile Dementia of Alzheimer Type and Vascular Dementia in Japan.	International Psychogeriatrics	15-2	322	2003

THE JOURNAL OF BIOLOGICAL CHEMISTRY
© 2004 by The American Society for Biochemistry and Molecular Biology, Inc.

Vol. 279, No. 11, Issue of March 12, pp. 10730–10737, 2004
Printed in U.S.A.

Munc13-4 Is a GTP-Rab27-binding Protein Regulating Dense Core Granule Secretion in Platelets*

Received for publication, August 25, 2003, and in revised form, December 16, 2003
Published, JBC Papers in Press, December 29, 2003, DOI 10.1074/jbc.M309426200

Ryutaro Shirakawa‡, Tomohito Higashi‡, Arata Tabuchi‡, Akira Yoshioka‡, Hiroaki Nishioka‡‡, Mitsunori Fukuda§, Toru Kita¶, and Hisanori Horiuchi‡‖**

From the Departments of ‡Geriatric Medicine and ¶Cardiovascular Medicine, Graduate School of Medicine, Kyoto University, Kyoto 606-8507, Japan and the §Fukuda Initiative Research Unit, RIKEN, Wako, Saitama 351-0198 Japan

Platelets store self-agonists such as ADP and serotonin in dense core granules. Although exocytosis of these granules is crucial for hemostasis and thrombosis, the underlying mechanism is not fully understood. Here, we show that incubation of permeabilized platelets with unprenylated active mutant Rab27A-Q78L, wild type Rab27A, and Rab27B inhibited the secretion, whereas inactive mutant Rab27A-T23N and other GTPases had no effects. Furthermore, we affinity-purified a GTP-Rab27A-binding protein in platelets and identified it as Munc13-4, a homologue of Munc13-1 known as a priming factor for neurotransmitter release. Recombinant Munc13-4 directly bound to GTP-Rab27A and -Rab27B *in vitro*, but not other GTPases, and enhanced secretion in an *in vitro* assay. The inhibition of secretion by unprenylated Rab27A was rescued by the addition of Munc13-4, suggesting that Munc13-4 mediates the function of GTP-Rab27. Thus, Rab27 regulates the dense core granule secretion in platelets by employing its binding protein, Munc13-4.

Upon stimulation, platelets secrete self-agonists, such as ADP and serotonin, which are stored in dense core granules (1). These secreted agonists contribute to the explosive activation of platelets in the processes of hemostasis and thrombus formation by a positive feedback mechanism (1). Despite this biological significance (1), the molecular mechanisms underlying this regulated exocytosis remain largely unclear.

Rab GTPases are essential regulatory molecules in vesicle transport (2, 3) and to date more than 50 members have been identified in mammals. Rab GTPases are localized to specific organelles and regulate several steps of vesicle transport including vesicle movement along cytoskeletal tracks and vesicle tethering to the target membrane by employing effector molecules that interact with GTP-bound Rab proteins (2, 3).

Recently, the *ashen* phenotype in mice has been demonstrated to be caused by a mutation in Rab27A (4). *Ashen* mice exhibit impaired coat color because of defective melanosome distribution, where Rab27A links a motor protein myosin Va and actin to melanosomes through its effector, melanophilin/Slac2-a (5–10). In addition, in cytotoxic T lymphocytes and natural killer cells in *ashen* mice, lytic granule secretion is impaired presumably at the docking/fusion step (11, 12). Interestingly, it has been demonstrated that the bleeding time of *ashen* mice is prolonged because of platelet dysfunction caused by a lack of intact platelet dense core granules (4, 13). However, it is important to note that platelets also contain Rab27B, a homologue of Rab27A with 71% identity in the amino acid level, which may compensate for the defect of Rab27A in platelets in *ashen* mice (14). These studies emphasize the requirement of further investigation into the mechanisms by which Rab27 may control the biogenesis and exocytosis of dense core granules in platelets.

The final step of vesicle transport is docking and fusion with the target membrane, which is mediated by *trans*-SNARE[1] complex between the vesicle SNARE and the target membrane SNARE (15). Accumulating evidence has revealed that Rab GTPases function upstream of SNARE pairing (2, 3). In addition to Rab GTPases, SNARE complex formation is directly regulated by several factors such as Munc18 and Munc13-1. In neuronal cells, Munc18 is thought to bind to the closed conformation of syntaxin1, a target membrane SNARE, to inhibit the *trans*-SNARE complex formation (16, 17). In contrast, Munc13-1 acts as a priming factor in neuronal secretion (18). Munc13-1 is suggested to promote formation of an open conformation of syntaxin1 and induce the assembly of *trans*-SNARE complexes. This is supported by the fact that transmission defects of *unc-13* mutants in *Caenorhabditis elegans* could be rescued by expression of open form of syntaxin (19). Munc13-1 and its homologues, Munc13-2 and Munc13-3, are expressed exclusively in brain, except for ubMunc13-2, a splicing variant of Munc13-2 (20, 21). In brain, each Munc13 isoform expression pattern is spatially restricted, although there is some overlap between isoforms. Munc13-1-deficient mice exhibit partial defects in glutamatergic neuron neurotransmitter release (22), whereas Munc13-1/Munc13-2 double knockout mice have complete loss of synaptic transmission in not only glutamatergic neurons but also GABAergic neurons (23). These studies in mice have revealed the essential and general roles of Munc13s in neurotransmitter release. Recently, the fourth Munc13 homologue, Munc13-4, was identified (24). In contrast to Munc13-1–3, Munc13-4 is expressed in non-neuronal tissues (24), and its biological function remains to be elucidated.

Here, we demonstrate that Rab27 regulates the Ca^{2+}-induced dense core granule secretion in platelets by showing that the addition of unprenylated Rab27 in an *in vitro* assay with permeabilized platelets inhibited the secretion. Furthermore, we identified a novel GTP-Rab27-binding protein in platelets as Munc13-4 and demonstrate that Munc13-4 mediates the function of GTP-Rab27 to promote the secretion.

* This work was supported by Ministry of Education, Culture, Sports, Science, and Technology Research Grants 11680629 and 15081101 (to H. H.) and 12CE2006, 09281104, and 13307034 (to T. K.), by Health and Labour Sciences Research Grant H14-Tyouju-012 from the Ministry of Health Labour and Welfare (to T. K. and H. H.), and in part by grants from the Takeda Science Foundation, Suzuken Memorial Foundation, the Study Group of Molecular Cardiology, and the Novartis Foundation for Gerontrogical Research (to H. H.). The costs of publication of this article were defrayed in part by the payment of page charges. This article must therefore be hereby marked "*advertisement*" in accordance with 18 U.S.C. Section 1734 solely to indicate this fact.

‖ To whom correspondence should be addressed. Tel.: 81-75-751-3464; Fax: 81-75-751-3574; E-mail: horiuchi@kuhp.kyoto-u.ac.jp.

** Present address: Department of Internal Medicine, Mitsubishi Kyoto Hospital, Kyoto, 615-8087 Japan.

‡‡ Present address: Sir William Dunn School of Pathology, University of Oxford, South Parks Rd., Oxford OX1 3RE, United Kingdom.

[1] The abbreviations used are: SNARE, soluble *N*-ethylmaleimide-sensitive factor attachment protein receptor; PKC, protein kinase C; SLO, streptolysin-O; GST, glutathione *S*-transferase; GTPγS, guanosine 5′-3-*O*-(thio)triphosphate; TOF-MS, time-of-flight mass spectrometry.

EXPERIMENTAL PROCEDURES

Antibodies, Constructs, Materials, and Others—Anti-Na,K-ATPase rabbit polyclonal antibody (25) was a kind gift from Dr. K. Omori (Kansai Medical University, Kadoma, Japan). Anti-His_6 and anti-PKCα monoclonal antibodies were purchased from Qiagen and Santa Cruz Biotechnology, respectively. Horseradish peroxidase-labeled anti-mouse and anti-rabbit IgG polyclonal antibodies were from Amersham Biosciences and were used as secondary antibodies for Western blot analysis visualized by enhanced chemiluminescence method (Amersham Biosciences). Unless otherwise specified, all of the other chemicals were purchased from Sigma, except for SLO, which was from Dr. S. Bhakdi (Mainz University, Mainz, Germany) (26).

The protein concentrations were determined by the Bradford method (Bio-Rad) or from the intensities of the bands in Coomassie Blue-stained SDS-PAGE gels using bovine serum albumin as a standard. cDNA encoding Rab27A was kindly provided by Dr. Y. Nozawa (Gifu International Institute of Biotechnology, Gifu, Japan) (27), and mutants Rab27A-Q78L and Rab27A-T23N were generated by PCR mutagenesis. cDNAs encoding Rap1B (28) and Rab3B (29) were from Dr. Y. Takai (Osaka University, Osaka, Japan), and Rab4B (30) and Rab5A (30) were from Dr. M. Zerial (Max Plank Institute, Dresden, Germany). Human Rab27B cDNA was isolated from the Marathon-Ready human bone marrow cDNA (Clontech) by PCR. All of these cDNAs were subcloned into the prokaryotic expression vector pDEST17 (Invitrogen) for His_6-tagged recombinant protein production. GST fusion proteins of Rab3B, Rab4B, Rab5A, Rab27A, and Rab27B were produced by subcloning the cDNAs into pGEX-2T (Amersham Biosciences). These His_6-tagged and GST fusion proteins were produced in *Escherichia coli* strain BL21 and purified on nickel-nitrilotriacetic acid-agarose (Qiagen) and glutathione-Sepharose (Amersham Biosciences), respectively. For full-length Munc13-4 recombinant protein production, the cDNA of Munc13-4 was subcloned into pDEST10 (Invitrogen), and a baculovirus encoding the full-length Munc13-4 was produced using the Bac-to-Bac system (Invitrogen). His_6-tagged Munc13-4 recombinant protein was produced in Sf9 insect cells upon infection with the virus and purified on nickel-nitrilotriacetic acid-agarose, followed by further purification with MonoQ anion exchange chromatography (Amersham Biosciences). All of the purified recombinant proteins were extensively dialyzed against buffer A (50 mM Hepes/KOH, pH 7.2, 78 mM KCl, 4 mM $MgCl_2$, 0.2 mM $CaCl_2$, 2 mM EGTA, 1 mM dithiothreitol) and stored at −80 °C until use. All of the sequences of the PCR products were confirmed by sequencing using a 3100 Genetic Analyzer (Applied Biosystems).

The Assay for Secretion of Dense Core Granules—The standard assay method for the Ca^{2+}-induced dense core granule secretion was essentially as described previously (31) except that human platelet cytosol was used (32) instead of rat brain cytosol. Unless otherwise specified, the standard assay was following: Freshly obtained washed platelets (1×10^8 platelets/assay, counted with the Coulter Counter) were incubated with [^{3}H]serotonin (~20,000 cpm/assay) (Amersham Biosciences) to allow uptake into dense core granules. After washing the platelets, the platelet plasma membrane was permeabilized with SLO in Buffer A, where the calculated free calcium ion concentration was ~20 nM (33). The permeabilized platelets were incubated with an ATP regeneration system, human platelet cytosol at 1.5 mg of proteins/ml (for Fig. 1) or 0.8 mg of proteins/ml (for Fig. 6), and tested materials at 4 °C for 30 min followed by further incubation at 30 °C for 2 min. Finally, the platelets were stimulated with 20 μM Ca^{2+} (33) at 30 °C for 1 min, and the reaction was stopped by the addition of ice-cold Buffer A containing 10 mM EGTA. After removing platelets by centrifugation, [^{3}H]serotonin released in the supernatant was measured by a liquid scintillation counter (Beckman). The secretion levels of [^{3}H]serotonin were expressed as percentages of the total [^{3}H]serotonin in the permeabilized platelets before the final incubation.

GST-Rab27A Affinity Column Chromatography—Human platelet pellets were provided by Kyoto Red Cross Blood Center and resuspended in Buffer A. After disruption of the platelets by sonication, the sample was centrifuged at 100,000 × *g* at 4 °C for 1 h. The supernatant was dialyzed against Buffer A and stored as human platelet cytosol at −80 °C until use. For the affinity chromatography, GTPγS- or GDP-bound GST-Rab27A was prepared by incubation of 30 μg of GST-Rab27A with 1 mM GTPγS or GDP in Buffer A containing 10 mM EDTA at 30 °C for 30 min, and the reaction was stopped by the addition of 15 mM $MgCl_2$ (34). Then the GST- or GST-Rab27A-coated beads were

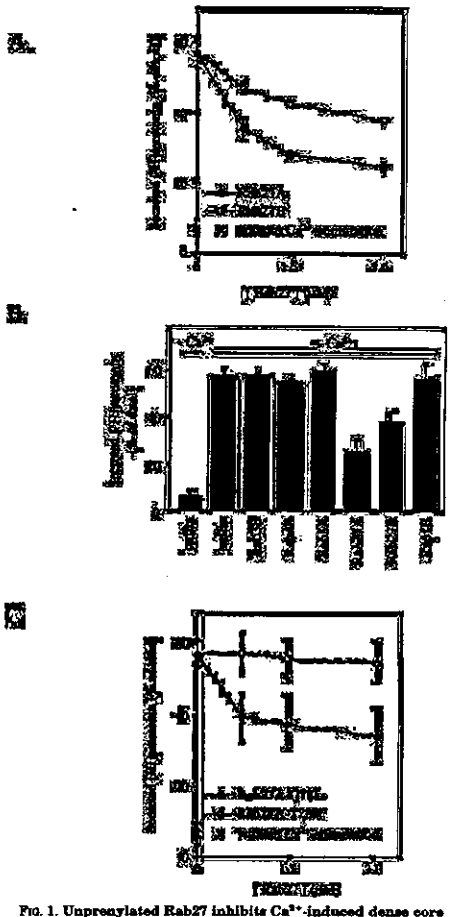

FIG. 1. **Unprenylated Rab27 inhibits Ca^{2+}-induced dense core granule secretion.** Permeabilized platelets were first incubated at 4 °C for 30 min with unprenylated His_6-Rab27A (*closed circles*) and His_6-Rab27B (*open circles*) purified from *E. coli* at various concentrations (*A*), with unprenylated His_6-Rab3B, -Rab4B, -Rab5A, -Rab27A, and -Rab27B and Rap1B at 3 μM (*B*), and with various concentrations of unprenylated mutant Rab27A-Q78L (*closed circles*) and Rab27A-T23N (*open circles*) (*C*). Then the Ca^{2+}-induced secretion of dense core granules was analyzed by measuring secreted [^{3}H]serotonin preloaded in dense core granules as described under "Experimental Procedures." The secretion without Ca^{2+} stimulation is also shown in *A* and *C* (×). The results shown are expressed as the means ± S.E. of three independent experiments.

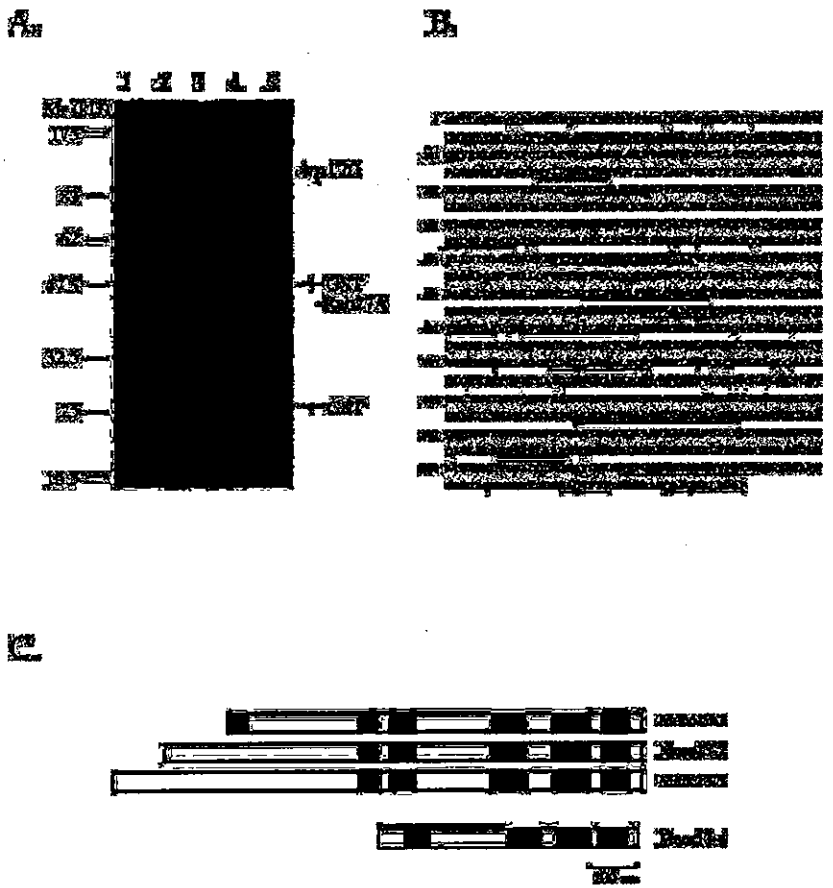

FIG. 2. **Identification of a GTP-Rab27A-binding protein in platelet cytosol as Munc13-4.** *A*, GST-loaded (*lane 3*) and GTPγS-bound (*lane 4*) and GDP-bound (*lane 5*) GST-Rab27A-loaded glutathione beads were incubated with platelet cytosol at 4 °C for 1 h. GST-loaded (*lane 1*) and GST-Rab27A-loaded (*lane 2*) beads were also treated in the same way without the cytosol. After washing the beads, the bead-associated proteins were analyzed in a Coomassie Blue-stained SDS-PAGE gel as described under "Experimental Procedures." A protein band at 120 kDa (*asterisk*) was specifically detected in *lane 4*. *B*, the 120-kDa protein was analyzed by TOF-MS and identified as human Munc13-4 as described under "Experimental Procedures." *Underlining* indicates the peptides whose masses were matched with peptide masses detected by the TOF-MS analysis. *C*, the domain structures of Munc13-1–3 and Munc13-4 are shown.

prepared by incubation of glutathione-Sepharose beads with GST or pretreated GST-Rab27A at 4 °C for 1 h, followed by washing the beads with Buffer A three times. The coated beads were incubated with the platelet cytosol (30 mg of proteins) at 4 °C for 1 h, followed by washing the beads with Buffer A three times, and the bead-associated proteins were extracted by the SDS sample buffer. The samples were analyzed in a Coomassie Blue-stained SDS-PAGE gel (4–20% gradient gel; Daiichi Chemical).

Cloning of Munc13-4—The TOF-MS analysis of the GTPγS-Rab27A-binding protein at 120 kDa was performed by Kyoto Science Co. (Kyoto, Japan). The report first showed that a candidate protein could be FLJ00067, which contained an incomplete sequence with possible introns and C-terminal deletion. We reconstituted the full-length sequence with several expressed sequence tags overlapping with FLJ00067 and identified it as a human homologue of rat Munc13-4 (24). Using the sequences, we designed primers and amplified the full-length cDNA by PCR using the Marathon-Ready human bone marrow cDNA (Clontech). The PCR product was cloned into pENTR (Invitrogen) and verified by sequencing using a 3100 Genetic Analyzer.

Anti-Munc13-4 and -Rab27 Antibodies—cDNA encoding the N-terminal region of Munc13-4 (residues 1–262) was obtained by PCR and subcloned into pDEST17 (Invitrogen). The His_6-Munc13-4 (1–262) protein was produced and purified as described above. Anti-Munc13-4 and anti-Rab27A rabbit polyclonal antibodies were generated using His_6-Munc13-4 (1–262) and His_6-Rab27A as antigens, respectively. The anti-Rab27A antibody recognized both Rab27A and Rab27B. For transient expression of Munc13-4, HeLa cells were transfected with pcDNA (Invitrogen) containing full-length Munc13-4 using LipofectAMINE (Invitrogen).

Assay Analyzing Direct Interaction of Munc13-4 with Rab27—Binding of Munc13-4 with small GTPases was carried out by affinity chromatography. Glutathione-Sepharose beads coated with GTPγS- or GDP-bound Rab GTPases (each 1 μg) were prepared by incubation for 1 h at 4 °C in Buffer A. Then the prepared beads were incubated with purified 0.5 μg of His_6-Munc13-4 for 1 h at 4 °C in Buffer A and washed three times with Buffer A at 4 °C. Bead-associated His_6-Munc13-4 was analyzed by immunoblotting with anti-Munc13-4 antibody.

Density Gradient Separation of Platelet Organelles—We first loaded [^{3}H]serotonin into dense core granules of platelets from 50 ml of freshly obtained blood and permeabilized the platelets with SLO. Then, after centrifugation to remove most of cytosol and resuspension in 1 ml of Buffer A containing the ATP regeneration system, the platelets were disrupted by sonication and centrifuged at 600 × *g* for 5 min to remove unbroken platelets. The supernatant was layered on the top of metrizamide stepwise gradient (each 1.0-ml layer at 1.30–1.00 g/ml in density decreasing by each 0.03 g/ml from the bottom) in Buffer A containing the ATP regeneration system and centrifuged at 28,000 rpm with Beckman Rotor *SW40* for 2 h at 4 °C as described (31). Aliquots of the fractions were analyzed by Western blot with indicated antibodies and counting radioactivity of [^{3}H]serotonin. The separation of the membrane and cytosolic fraction was performed by centrifugation at 300,000 × *g* for 30 min at 4 °C after disrupting platelets by sonication or at 600 × *g* for 5 min after the SLO permeabilization of platelets.

RESULTS

Unprenylated Rab27 Inhibits the Ca^{2+}-induced Dense Core Granule Secretion—In the present study, we used a previously established *in vitro* assay system using SLO-permeabilized platelets by monitoring secreted [^{3}H]serotonin preloaded into dense core granules (31, 32, 35). Agonists promote granule secretions by increasing intracellular calcium ion concentrations in platelets (36). Upon permeabilization of platelets the intracellular and extracellular concentrations of calcium are equal; therefore we used calcium chloride as a stimulus. In the assay, the secretion of the granules was reconstituted by the addition of ATP and exogenous platelet cytosol, and the response obeerved was equivalent to intact platelets in the time course and the Ca^{2+} sensitivity (31, 32, 35).

Small GTPases produced in *E. coli* are not modified by the addition of prenyl groups at their C termini (37), which is essential for the correct localization and activity (2, 3, 38). Incubation of permeabilized platelets with Rab27A and Rab27B purified from *E. coli* inhibited the Ca^{2+}-induced dense core granule secretion in a concentration-dependent manner (Fig. 1*A*). Incubation of permeabilized platelets with other small GTPases such as Rab3B, Rab4B, Rab5A, or Rap1B, a Ras family small GTPase whose GTP-bound form has been shown to be increased upon platelet activation (39), had no effect (Fig. 1*B*), indicating that the effect of Rab27 is specific. We prepared and purified mutant Rab27A-T23N, which preferentially binds GDP, and Rab27A-Q78L, which lacks GTPase activity (40). Incubation of permeabilized platelets with Rab27A-Q78L, but not Rab27A-T23N, inhibited the secretion in a concentration-dependent manner (Fig. 1*C*). Inhibition by unprenylated Rab27A-Q78L, wild type Rab27A, and Rab27B could be due to sequestration of putative Rab27 effector molecules from endogenous membrane-associated GTP-Rab27 by forming nonfunctional complexes with effector proteins. These data demonstrate that Rab27 is involved in the regulation of dense core granule secretion in platelets.

Identification of Munc13-4 as a GTP-Rab27-binding Protein in Platelet Cytosol—To elucidate the mechanism of action of Rab27, we attempted to identify GTP-Rab27-binding proteins that might mediate the function of Rab27 in the granule secretion, from platelet cytosol by affinity chromatography. As shown in Fig. 2*A*, we detected one major protein migrating at ~120 kDa on GTPγS-GST-Rab27A beads (*lane 4*) but not on GDP-GST-Rab27A- (lane 5) or GST beads (*lane 3*). TOF-MS analysis of the protein and a data base search revealed that the 120-kDa protein was the human homologue of rat Munc13-4 (24) because most of the peptide masses obtained by the TOF-MS analysis were detected all over the human Munc13-4 molecule (Fig. 2*B*). Human Munc13-4 consists of 1,090 amino acids, and the primary structure is 88% identical to that of rat Munc13-4. As is the case with Munc13-1–3, Munc13-4 contains two calcium-binding C2 domains and Munc13 homology do-

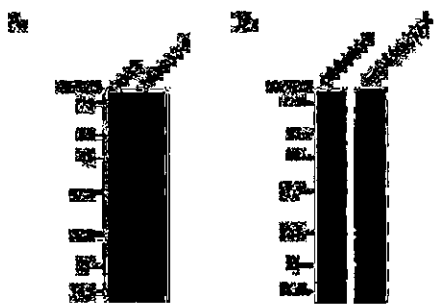

FIG. 3. **Anti-Munc13-4 antibody recognizes a single band at 120 kDa in platelet lysate.** *A*, Munc13-4- and mock-transfected HeLa cell lysates were immunoblotted with the anti-Munc13-4 antibody as described under "Experimental Procedures." *B*, platelet lysates were immunoblotted with preimmune serum and the anti-Munc13-4 antibody as described under "Experimental Procedures." The data shown are the representative of three independent experiments with similar results.

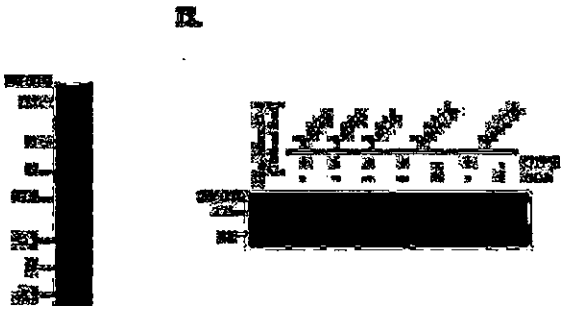

FIG. 4. **Direct interaction of recombinant Munc13-4 with GTPγS-Rab27 *in vitro*.** *A*, recombinant His_6-Munc13-4 was produced and purified from the over-expressing Sf9 cells and analyzed by SDS-PAGE gel stained by Coomassie Blue as described under "Experimental Procedures." *B*, glutathione beads coated with GTPγS- or GDP-bound various GST-Rab GTPases (each 1 μg) were incubated with His_6-Munc13-4 (0.5 μg) *in vitro*, and the bead-associated His_6-Munc13-4 was detected by Western blotting with anti-His_6 antibody as described under "Experimental Procedures." Purified Munc13-4 used for the affinity analysis is also shown (10% of load). The data shown are representative of three independent experiments with similar results.

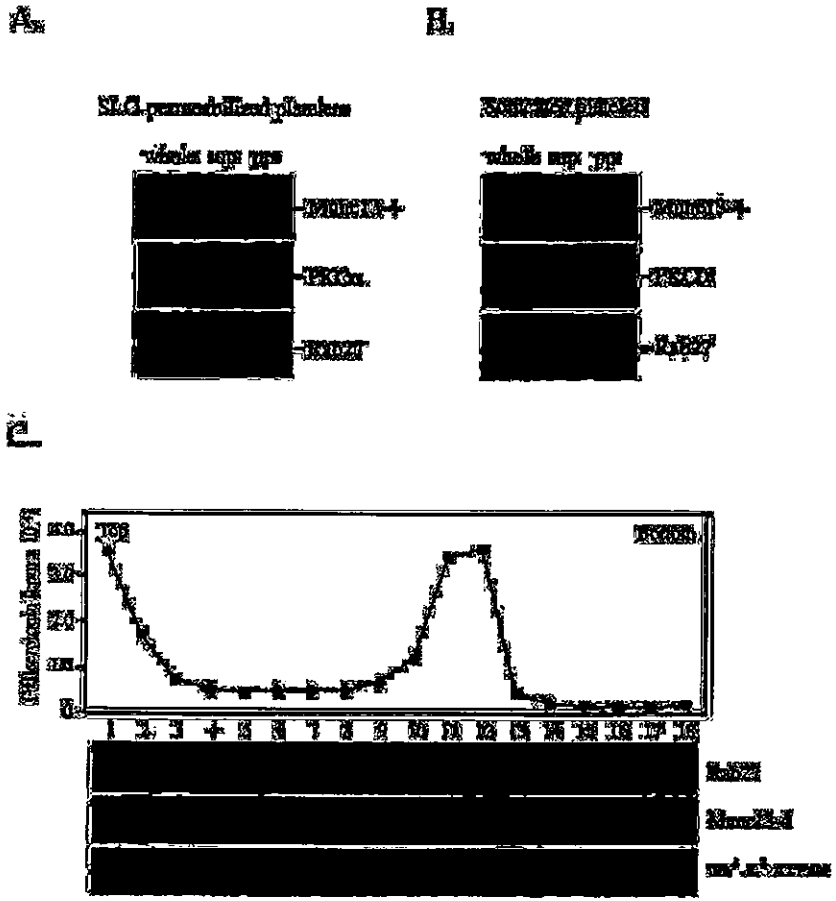

FIG. 5. **Localization of Munc13-4 in platelet organelles.** *A* and *B*, after centrifugation of isolated platelets permeabilized with SLO for 30 min (*A*) or sonicated directly (*B*), comparable amounts of the supernatant (*sup*) and pellets (*ppt*) were analyzed by immunoblotting with anti-Munc13-4, anti-PKCα, and anti-Rab27 antibodies as described under "Experimental Procedures." The data shown are the representative of three independent experiments with similar results. *C*, after separation of organelles of [^{3}H]serotonin-loaded permeabilized platelets by density gradient, [^{3}H]serotonin was measured by a liquid scintillation counter and Munc13-4, Rab27, and Na,K-ATPase were detected by immunoblotting in each fraction as described under "Experimental Procedures." The data shown are the representative of three independent experiments with similar results.

mains, whereas Munc13-4 lacks the long N-terminal region containing a phorbol ester-binding C1 domain present in Munc13-1–3 (21, 24) (Fig. 2*C*).

We generated an antibody against the N-terminal region of human Munc13-4 (residues 1–262). The antibody recognized a 120-kDa protein in HeLa cells transfected with Munc13-4 but not in mock transfected cells (Fig. 3*A*). The antibody recognized a single band at 120 kDa in platelet lysate (Fig. 3*B*) and also the 120-kDa protein eluted from the GTPγS-GST-Rab27A-loaded affinity chromatography column (data not shown), confirming that the 120-kDa protein that we identified is indeed Munc13-4.

To examine whether the interaction of Munc13-4 with Rab27 is direct, we produced and purified full-length His_6-Munc13-4 using the baculovirus expression system in Sf9 insect cells (Fig. 4*A*). As shown in Fig. 4*B*, recombinant Munc13-4 could bind directly to GTPγS-Rab27A but only slightly to GDP-Rab27A *in vitro*. Furthermore, Munc13-4 demonstrated a weaker interaction with GTPγS-Rab27B, compared with GTPγS-Rab27A. Importantly, Munc13-4 did not bind to GTPγS-Rab3B, -Rab4B, or -Rab5A (Fig. 4*B*). Thus, the interaction of Munc13-4 with Rab27 is direct, GTP-dependent, and specific.

Localization of Munc13-4—Munc13-1 has been demonstrated to localize specifically to the presynaptic plasma membrane, although it does not contain a membrane-spanning region (20). Munc13-4 also lacks a transmembrane region. We examined the subcellular localization of Munc13-4 in platelets. As shown in Fig. 5*A*, Munc13-4 was equally distributed between the cytosolic and membrane fractions in SLO-permeabilized platelets, whereas Rab27 was exclusively membrane-associated. As expected, PKCα was found predominantly in the soluble supernatant fraction (Fig. 5*A*). When isolated platelets were directly sonicated and centrifuged at 300,000 × *g*, localization of Munc13-4, Rab27, and PKCα was similar to the results in the SLO-permeabilized platelets (Fig. 5*B*). Namely, ~50% of Munc13-4, most of Rab27, and a small part of PKCα were recovered in the pellet after the high speed centrifugation (Fig. 5*B*), suggesting a strong affinity of Munc13-4 to the membrane.

Next, we biochemically examined the localization of Rab27 and membrane-associated Munc13-4 in platelet organelles. We first loaded [^{3}H]serotonin into dense core granules of platelets and permeabilized the platelets with SLO. Then, after centrifugation to remove cytosol, the cytosol-depleted platelets were disrupted by sonication, and the low speed supernatant containing platelet organelles was separated by a density gradient method (31). As shown in Fig. 5*C*, [^{3}H]serotonin was recovered in two peaks. The lighter peak is presumably due to [^{3}H]serotonin leaking from the dense core granules. The heavier fractions of [^{3}H]serotonin indicate the presence of dense core granules. The majority of Rab27 was recovered together with fractions of dense core granules containing [^{3}H]serotonin, whereas some Rab27 was detected in the low density fractions where a plasma membrane marker Na,K-ATPase was recovered (Fig. 5*C*). Under these conditions, Munc13-4 was recovered in the lighter fractions together with Na,K-ATPase but not in the vesicle fractions (Fig. 5*C*), suggesting that Munc13-4 is on the plasma membrane but not on the dense core granules in platelets.

Involvement of Munc13-4 in the Regulation of Dense Core Granule Secretion—We finally examined whether Munc13-4 regulates dense core granule secretion in platelets using the semi-intact secretion assay. In basal conditions, SLO-permeabilized platelets retained a residual amount of membrane-associated Munc13-4 (Fig. 5*A*), and exogenously added platelet cytosol contained 60 nM Munc13-4. Under these conditions, the addition of purified Munc13-4 (Fig. 4*A*) enhanced the Ca^{2+}-induced secretion of dense core granules in a concentration-dependent manner (Fig. 6*A*). The activity of Munc13-4 was abolished when Munc13-4 was denatured (Fig. 6*A*), suggesting that the activity was not due to a nonspecific effect of the buffer. The dense core granule secretion was time-dependent, and the addition of Munc13-4 not only accelerated the kinetics but also increased the amounts of the secretion (Fig. 6*B*). Importantly, the inhibition of secretion by unprenylated Rab27A was rescued by the addition of recombinant Munc13-4 in a concentration-dependent manner (Fig. 6*C*).

DISCUSSION

Here we have demonstrated that Rab27 regulates the Ca^{2+}-induced dense core granule secretion in platelets by showing that the addition of unprenylated dominant active Rab27A, wild type Rab27A, and Rab27B but not other GTPases inhibited the secretion in permeabilized platelets. In addition, we identified Munc13-4 as a novel GTP-Rab27-binding protein. We further demonstrated that Munc13-4 mediates the function of GTP-Rab27 in the regulation of the secretion by showing that the addition of Munc13-4 enhanced the secretion and rescued the inhibition of secretion by unprenylated Rab27.

We have shown that the addition of unprenylated Rab27 purified from *E. coli* inhibited the Ca^{2+}-induced dense core granule secretion. In the secretion assay, added unprenylated Rab27 is theoretically unable to localize to the membrane and therefore would sequester Rab27 effector molecules by forming

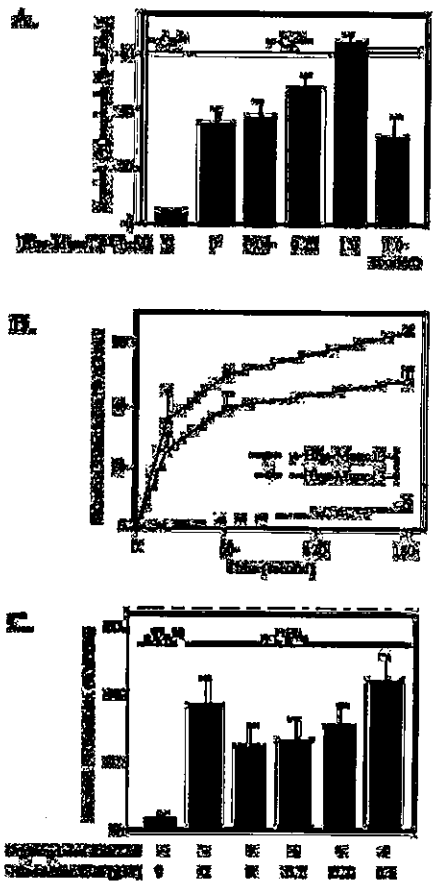

FIG. 6. **Munc13-4 enhances the dense core granule secretion and rescues the inhibition by unprenylated Rab27A.** *A*, permeabilized platelets were first incubated with the indicated concentrations of Munc13-4, and the Ca^{2+}-induced secretion of dense core granules for 1 min was analyzed in the standard assay condition by measuring secreted [^{3}H]serotonin preloaded in dense core granules as described under "Experimental Procedures." *B*, permeabilized platelets were first incubated in the absence (*open circles*) or the presence (*closed circles*) of 0.2 μM Munc13-4 and then incubated with Ca^{2+} at 20 nM (*broken lines*) or 20 μM (*solid lines*) for the indicated periods. The Ca^{2+}-induced secretion of dense core granules for indicated periods was analyzed as described under "Experimental Procedures." *C*, permeabilized platelets were first incubated in the absence or presence of unprenylated Rab27A at 2.0 μM with various concentrations of Munc13-4. The Ca^{2+}-induced secretion of dense core granules for 1 min was analyzed as described under "Experimental Procedures." The results shown are expressed as the means ± S.E. of three independent experiments.

nonfunctional complexes. Unprenylated Rab27A-T23N with preferential GDP binding would act as a dominant negative protein when expressed in cells (41). However, here we observed almost no effect of Rab27A-T23N on the dense core granule secretion in our semi-intact system (Fig. 1*C*). On the other hand, unprenylated GTPase-deficient mutant Rab27A-Q78L inhibited the secretion to a similar extent as wild type Rab27A and Rab27B. This could depend upon the ability of association with effector molecules of Rab27. The mechanism might be similar to that seen in the inhibition of the insulin signaling in adipocytes by overexpression of prenylation-deficient Rab4 (42). Thus, GTP-Rab27 is essential for dense core granule secretion in platelets once the granules are normally generated, although there is controversy concerning the role of Rab27 in dense core granule biogenesis (4, 13, 14).

To identify specific GTP-Rab27-binding protein(s) that may function in dense core granule secretion in platelets, we performed Rab27 affinity chromatography using platelet cytosol as the source for interacting proteins. We detected a GTPγS-Rab27A-binding protein at 120 kDa and identified it as the human homologue of rat Munc13-4 (24) by TOF-MS analysis and a data base search. Recombinant Munc13-4 bound to purified Rab27A and Rab27B in their GTPγS-bound forms *in vitro*, indicating that their interaction is direct and nucleotide-dependent.

So far, eight proteins have been identified as GTP-Rab27A-binding molecules (43, 44). Five of them contain the C-terminal tandem calcium-binding C2 domains (45) and are designated as synaptotagmin-like proteins (Slp 1–5) (43, 44). The other three are homologous to Slps but lack the C2 domains and are designated as Slp-lacking C2 domains (Slac2-a–c) (43). All of these molecules contain the Slp homology domain at their N-terminal ends, through which these molecules interact directly with GTP-Rab27 (43). Munc13-4 does not contain this Slp homology domain motif (43, 44). Therefore, we conclude that Munc13-4 is a novel type of GTP-Rab27-binding molecule.

We have demonstrated that the addition of recombinant Munc13-4 in the secretion assay accelerated the kinetics and increased secretion, indicating that Munc13-4 positively regulates dense core granule secretion in platelets. Importantly, the inhibitory effect of unprenylated Rab27A was rescued by the addition of recombinant Munc13-4. Exogenously added unprenylated Rab27A is presumed to form nonfunctional complexes with putative Rab27 effectors, thereby inhibiting secretion. Because exogenously added Munc13-4 overcomes inhibition by unprenylated Rab27, it is most likely that Munc13-4 mediates the function of GTP-Rab27 in the dense core granule secretion in platelets. Interestingly, the inhibitory effect of unprenylated Rab27A on the secretion was stronger than that of unprenylated Rab27B (Fig. 1*A*), which may reflect distinct roles of each isoform within the regulation of dense core granule secretion in platelets. Our data suggest that this difference is due to the stronger affinity of Rab27A to Munc13-4 than that of Rab27B (Fig. 4*B*).

Because SNAREs and Rab GTPases are key molecules in the regulation of vesicle transport, elucidation of the molecular mechanism of their cooperation could provide a clue for further understanding of vesicle docking/fusion. There have been several examples of Rab effector proteins interacting with the components of the SNARE machinery. For example, the Rab5 effector Rabenosyn-5 interacts directly with Vps45, a member of the Munc18/Sec1 family, in the regulation of endocytic membrane traffic (46). Similarly, the Ypt7 effector complex that controls vacuolar fusion in yeast interacts directly with Vps33, which is also a Munc18/Sec1 family protein (47). Thus, a group of Rab effectors appear to regulate SNARE pairing through Munc18/Sec1 family proteins. Another group of Rab effectors has been shown to bind SNAREs directly, as shown for the Rab5 effector EEA1 interacting with syntaxin6 (48) and syntaxin13 (49).

It has also been demonstrated that Munc13-1 could be a direct regulator of syntaxin1 (50, 51) and that a GTP-Rab3A-binding protein, RIM1, which is a cytomatrix protein at the active zone in synapses, interacts with Munc13-1 (52). Thus, Rab3A might regulate Munc13-1 indirectly through interaction with RIM1. On the other hand, we here report the first direct link between Rab GTPases and a member of the Munc13 family, which may provide a novel mechanism for the control of SNARE activity by regulatory Rab GTPases. It will now be essential to explore the mechanisms of how Munc13-4 regulates the SNARE pairs that function in dense core granule secretion. In platelets, it has been shown that syntaxin2 mediates dense core granule secretion (53), suggesting that Munc13-4 might regulate syntaxin2.

We detected Munc13-4 in both cytosolic and membrane fractions, whereas Rab27 is exclusively in the membrane fraction (Fig. 5, *A* and *B*). Furthermore, by a density gradient separation, Munc13-4 was recovered in the plasma membrane fraction, whereas a major part of Rab27 was recovered in the granule fraction (Fig. 5*C*). Thus, the localization of Rab27 and Munc13-4 is not overlapping to a great extent. Munc13-4 on the plasma membrane may mark the target site for the dense core granule docking by interacting directly with activated Rab27 on the vesicle membrane. Because Rab3A is present on the synaptic vesicles (54) and its effector RIM1 and RIM1's partner Munc13-1 are on the presynaptic membrane in neurons (20), there might be a common regulatory mechanism used by the Rab GTPase-Munc13 system.

Taken together, the work presented here demonstrates that Rab27 regulates dense core granule secretion in platelets by employing the GTP-Rab27-binding protein, Munc13-4. Our current findings could provide a novel mechanism by which a Rab GTPase controls the regulated exocytosis through direct interaction with a Munc13 family protein. To contribute to further understanding of the regulation of vesicle transport, it is essential to elucidate the molecular mechanism of how the Rab27-Munc13-4 system promotes regulated exocytosis.

Acknowledgments—We are grateful to Dr. M. Zerial for providing plasmids containing Rab4 and Rab5, Dr. Y. Nozawa for a plasmid containing Rab27A, Dr. Y. Takai for a plasmid containing Rap1B and Rab3B, and Dr. K. Omori for providing an anti-Na,K-ATPase antibody. We are also grateful to the Kyoto Red Cross Blood Center for providing platelet pellets. We thank Dr. H. McBride (Ottawa, Canada) and Dr. C. Murphy (Ioannina, Greece) for critical reading of the manuscript and T. Matsubara for excellent technical assistance.

Note Added in Proof—Feldmann *et al.* (Feldmann, J., Callebaut, I., Raposo, G., Certain, S., Bacq, D., Dumont, C., Lambert, N., Ouachee-Chardin, M., Chedeville, G., Tamary, H., Minard-Colin, V., Vilmer, E., Blanche, S., Le Deist, F., Fisher, A., and de Saint Basile, G. (2003) *Cell* 115, 461–473) have published that mutation in Munc13-4 causes familial hemophagocytic lymphohistiocytosis (FHL3) where cytolytic granule fusion to the plasma membrane in cytotoxic T lymphocytes is impaired similar to mutation in Rab27A (11, 12), suggesting that the Rab27-Munc13-4 regulatory system may also function in regulated secretion in the cells.

REFERENCES

1. Brass, L. F. (2000) in *Hematology: Basic Principles and Practice* (Hoffman, R. S., Benz, E. J., Furie, B., Cohen, H., and Silberstein, L. E., ed) 3rd Ed., pp. 1753–1770, Churchill Livingston, New York
2. Takai, Y., Sasaki, T., and Matozaki, T. (2001) *Physiol. Rev.* 81, 153–208
3. Zerial, M., and McBride, H. (2001) *Nat. Rev. Mol. Cell Biol.* 2, 107–117
4. Wilson, S. M., Yip, R., Swing, D. A., O'Sullivan, T. N., Zhang, Y., Novak, E. K., Swank, R. T., Russell, L. B., Copeland, N. G., and Jenkins, N. A. (2000) *Proc. Natl. Acad. Sci. U. S. A.* 97, 7933–7938
5. Wu, X. S., Rao, K., Zhang, H., Wang, F., Sellers, J. R., Matesic, L. E., Copeland, N. G., Jenkins, N. A., and Hammer, J. A., III (2002) *Nat. Cell Biol.* 4, 271–278
6. Huma, A. N., Collinson, L. M., Hopkins, C. R., Strom, M., Barral, D. C., Bossi, G., Griffiths, G. M., and Seabra, M. C. (2002) *Traffic* 3, 193–202
7. Provance, D. W., James, T. L., and Mercer, J. A. (2002) *Traffic* 3, 124–132
8. Fukuda, M., Kuroda, T. S., and Mikoshiba, K. (2002) *J. Biol. Chem.* 277, 12432–12436
9. Nagashima, K., Torii, S., Yi, Z., Igarashi, M., Okamoto, K., Takeuchi, T., and Izumi, T. (2002) *FEBS Lett.* 517, 233–238
10. Kuroda, T. S., Ariga, H., and Fukuda, M. (2003) *Mol. Cell Biol.* 23, 5246–5255
11. Stinchcombe, J. C., Bossi, G., Booth, S., and Griffiths, G. M. (2001) *Immunity* 15, 751–761
12. Haddad, E. K., Wu, X., Hammer, J. A., III, and Henkart, P. A. (2001) *J. Cell Biol.* 153, 835–842
13. Novak, E. K., Gautam, R., Reddington, M., Collinson, L. M., Copeland, N. G., Jenkins, N. A., McGarry, M. P., and Swank, R. T. (2002) *Blood* 100, 128–135
14. Barral, D. C., Ramalho, J. S., Anders, R., Hume, A. N., Knapton, H. J., Tolmachova, T., Collinson, L. M., Goulding, D., Anthi, K. S., and Seabra, M. C. (2002) *J. Clin. Invest.* 110, 247–257
15. Chen, Y. A., and Scheller, R. H. (2001) *Nat. Rev. Mol. Cell Biol.* 2, 98–106
16. Dulubova, I., Sugita, S., Hill, S., Hosaka, M., Fernandez, I., Sudhof, T. C., and Rizo, J. (1999) *EMBO J.* 18, 4372–4382
17. Yang, B., Steegmaier, M., Gonzalez, L. C., Jr., and Scheller, R. H. (2000) *J. Cell Biol.* 148, 247–252
18. Ashery, U., Varoqueaux, F., Voets, T., Betz, A., Thakur, P., Koch, H., Neher, E., Brose, N., and Rettig, J. (2000) *EMBO J.* 19, 3586–3596
19. Richmond, J. E., Weimer, R. M., and Jorgensen, E. M. (2001) *Nature* 412, 338–341
20. Brose, N., Hofmann, K., Hata, Y., and Sudhof, T. C. (1995) *J. Biol. Chem.* 270, 25273–25280
21. Augustin, I., Betz, A., Herrmann, C., Jo, T., and Brose, N. (1999) *Biochem. J.* 337, 363–371
22. Augustin, I., Rosenmund, C., Sudhof, T. C., and Brose, N. (1999) *Nature* 400, 457–461
23. Varoqueaux, F., Sigler, A., Rhee, J. S., Brose, N., Enk, C., Reim, K., and Rosenmund, C. (2002) *Proc. Natl. Acad. Sci. U. S. A.* 99, 9037–9042
24. Koch, H., Hofmann, K., and Brose, N. (2000) *Biochem. J.* 349, 247–253
25. Akayama, M., Nakada, H., Omori, K., Masaki, R., Taketani, S., and Tushiro, Y. (1986) *Cell Struct. Funct.* 11, 259–271
26. Palmer, M., Harris, R., Freytag, C., Kehoe, M., Tranum-Jensen, J., and Bhakdi, S. (1998) *EMBO J.* 17, 1598–1605
27. Nagata, K., Satoh, T., Itoh, H., Kozasa, T., Okano, Y., Doi, T., Kaziro, Y., and Nozawa, Y. (1990) *FEBS Lett.* 275, 29–32
28. Matsui, Y., Kikuchi, A., Kawata, M., Kondo, J., Teranishi, Y., and Takai, Y. (1990) *Biochem. Biophys. Res. Commun.* 166, 1010–1016
29. Matsui, Y., Kikuchi, A., Kondo, J., Hishida, T., Teranishi, Y., and Takai, Y. (1988) *J. Biol. Chem.* 263, 11071–11074
30. Chavrier, P., Vingron, M., Sander, C., Simons, K., and Zerial, M. (1990) *Mol. Cell Biol.* 10, 6578–6585
31. Shirakawa, R., Yoshioka, A., Horiuchi, H., Nishioka, H., Tabuchi, A., and Kita, T. (2000) *J. Biol. Chem.* 275, 33844–33849
32. Yoshioka, A., Shirakawa, R., Nishioka, H., Tabuchi, A., Higashi, T., Ozaki, H., Yamamoto, A., Kita, T., and Horiuchi, H. (2001) *J. Biol. Chem.* 276, 39379–39385
33. Fabiato, A., and Fabiato, F. (1979) *J. Physiol. (Paris)* 75, 463–505
34. Christoforidis, S., McBride, H. M., Burgoyne, R. D., and Zerial, M. (1999) *Nature* 397, 621–625
35. Yoshioka, A., Horiuchi, H., Shirakawa, R., Nishioka, H., Tabuchi, A., Higashi, T., Yamamoto, A., and Kita, T. (2001) *Ann. N. Y. Acad. Sci.* 947, 403–406
36. Knight, D. E., and Scrutton, M. C. (1980) *Thromb. Res.* 20, 437–446
37. Nordfer, C., Peter, F., and Baleh, W. E. (1995) *Methods Enzymol.* 257, 3–9
38. Pereira-Leal, J. B., Hume, A. N., and Seabra, M. C. (2001) *FEBS Lett.* 498, 197–200
39. Franke, B., Akkerman, J. W., and Bos, J. L. (1997) *EMBO J.* 16, 252–259
40. Menasche, G., Feldmann, J., Houdusse, A., Desaymard, C., Fischer, A., Goud, B., and de Saint Basile, G. (2003) *Blood* 101, 2736–2742
41. Hume, A. N., Collinson, L. M., Rapak, A., Gomes, A. Q., Hopkins, C. R., and Seabra, M. C. (2001) *J. Cell Biol.* 152, 795–808
42. Knight, J. B., Cao, K. T., Gibson, G. V., and Olson, A. L. (2000) *Endocrinology* 141, 208–218
43. Kuroda, T. S., Fukuda, M., Ariga, H., and Mikoshiba, K. (2002) *J. Biol. Chem.* 277, 9212–9218
44. Kuroda, T. S., Fukuda, M., Ariga, H., and Mikoshiba, K. (2002) *Biochem. Biophys. Res. Commun.* 293, 899–906
45. Newton, A. C., and Johnson, J. E. (1998) *Biochim. Biophys. Acta* 1376, 155–172
46. Nielsen, E., Christoforidis, S., Uttenweiler-Joseph, S., Miaczynska, M., Dewitte, F., Wilm, M., Hoflack, B., and Zerial, M. (2000) *J. Cell Biol.* 151, 601–612
47. Price, A., Seals, D., Wickner, W., and Ungermann, C. (2000) *J. Cell Biol.* 148, 1231–1238
48. Simonsen, A., Gaullier, J. M., D'Arrigo, A., and Stenmark, H. (1999) *J. Biol. Chem.* 274, 28857–28860
49. McBride, H. M., Rybin, V., Murphy, C., Giner, A., Teasdale, R., and Zerial, M. (1999) *Cell* 98, 377–386
50. Sassa, T., Harada, S., Ogawa, H., Rand, J. B., Maruyama, I. N., and Hosono, R. (1999) *J. Neurosci.* 19, 4772–4777
51. Brose, N., Rosenmund, C., and Rettig, J. (2000) *Curr. Opin. Neurobiol.* 10, 303–311
52. Schoch, S., Castillo, P. E., Jo, T., Mukherjee, K., Geppert, M., Wang, Y., Schmitz, F., Malenka, R. C., and Sudhof, T. C. (2002) *Nature* 415, 321–326
53. Chen, D., Bernstein, A. M., Lemons, P. P., and Whiteheart, S. W. (2000) *Blood* 95, 921–929
54. Matteoli, M., Takei, K., Cameron, R., Hurlbut, P., Johnston, P. A., Sudhof, T. C., Jahn, R., and De Camilli, P. (1991) *J. Cell Biol.* 115, 625–633

THE JOURNAL OF BIOLOGICAL CHEMISTRY
Vol. 279, No. 19, Issue of May 7, pp. 19816–19823, 2004
Printed in U.S.A.

Advanced Glycation End Products Increase Collagen-specific Chaperone Protein in Mouse Diabetic Nephropathy*

Received for publication, September 22, 2003, and in revised form, February 24, 2004
Published, JBC Papers in Press, March 5, 2004, DOI 10.1074/jbc.M310428200

Seiji Ohashi‡, Hideharu Abe‡, Toshikazu Takahashi‡, Yasuhiko Yamamoto§, Masayoshi Takeuchi¶, Hidenori Arai‖, Kazuhiro Nagata, Toru Kita‡‡, Hiroshi Okamoto§§, Hiroshi Yamamoto§, and Toshio Doi‡¶¶**

*From the ‡Department of Clinical Biology and Medicine, Course of Biological Medicine, School of Medicine, The University of Tokushima, Tokushima 770-8503, Japan, §Department of Biochemistry and Molecular Vascular Biology, Kanazawa University Graduate School of Medical Science, Kanazawa 920-8640, Japan, ¶Department of Biochemistry, Faculty of Pharmaceutical Science, Hokuriku University, Kanazawa 920-1181, Japan, ‖Department of Geriatric Medicine, **Department of Molecular and Cellular Biology, Institute for Frontier Medical Sciences, ‡‡Department of Cardiovascular Medicine, Kyoto University, Kyoto 606-8575, Japan, and §§Department of Biochemistry, Tohoku University Graduate School of Medicine, Sendai 980-8575, Japan*

Advanced glycation end products (AGEs) appear to contribute to the diabetic complications. This study reports the inhibitory effect of OPB-9195 (OPB), an inhibitor of AGEs formation, and the role of a collagen-specific molecular chaperone, a 47-kDa heat shock protein (HSP47) in diabetic nephropathy. Transgenic mice carrying nitric-oxide synthase cDNA fused with insulin promoter (iNOSTg) leads to diabetes mellitus. The iNOSTg mice at 6 months of age represented diffuse glomerulosclerosis, and the expression of HSP47 was markedly increased in the mesangial area in parallel with increased expression of types I and IV collagens. OPB treatment ameliorated glomerulosclerosis in the iNOSTg mice associated with the decreased expression of HSP47 and types I and IV collagens. The expression of transforming growth factor-β (TGF-β) was increased in glomeruli of iNOSTg mice and decreased after treatment with OPB. To confirm these mechanisms, cultured mesangial cells were stimulated with AGEs. AGEs significantly increased the expression of HSP47, type IV collagen, and TGF-β mRNA. Neutralizing antibody for TGF-β inhibited the overexpression of both HSP47 and type IV collagen *in vitro*. In conclusion, AGEs increase the expression of HSP47 in association with collagens, both *in vivo* and *in vitro*. The processes may be mediated by TGF-β.

Nephropathy is a morbid complication associated with diabetes mellitus and is the leading cause of end-stage renal disease (1). Diabetic nephropathy is characterized by a mesangial expansion followed by glomerulosclerosis. The mechanism of these processes remains unknown. Advanced glycation end products (AGEs)[1] have been recently reported to play an important role in the pathogenesis of diabetic complications, particularly in the progression of retinopathy and nephropathy (2). AGEs, late compounds formed from early Amadori compounds produced during the Maillard reaction, slowly accumulate in various tissues. Direct evidence indicating the importance of AGEs in the progression of diabetic nephropathy has been reported previously (3–5). The administration of exogenous AGEs to normal rats induces glomerular hypertrophy and mesangial sclerosis, gene expression of matrix proteins, and production of various growth factors. An inhibitor of AGEs formation, aminoguanidine, ameliorates the mild glomerular changes and functional changes found in streptozocin-induced diabetic rats (6). Recently, a synthetic thiazolidine derivative, OPB-9195, was shown to have a strong inhibitory effect of AGE formation (7).

The 47-kDa heat shock protein (HSP47) has been identified as a collagen-binding stress protein and plays a role in the intracellular processing of procollagen molecules as a collagen-specific molecular chaperone. We recently reported that the expression of HSP47 was markedly increased in parallel with the development of glomerulosclerosis in a rat renal ablation model (8). We also found that the inhibition of HSP47 ameliorated glomerulosclerosis (9). Despite a possible pathophysiological role of collagen-binding HSP47 in the fibrotic process in various organs, factors that modulate its expression remain undefined.

To understand the pathogenesis of diabetic nephropathy and to develop prophylactic and therapeutic measures against it, suitable animal models are needed. However, no single animal model that develops the renal changes seen in humans is available. Spontaneously diabetic animals such as the non-obese diabetic mouse develop only limited lesions, at most mild mesangial sclerosis (10). The same is the case with chemically induced diabetic rodents. In this study, we analyzed transgenic mice carrying the mouse, type 2-inducible nitric-oxide synthase (iNOS) cDNA under the control of an insulin promoter (iNOSTg) (11). The nitric oxide-mediated destruction of β cells results in a markedly reduced pancreatic islet mass and in the development of type 1 diabetes mellitus. These characteristics were followed by glomerulosclerosis that resembled human diabetic nephropathy (3).

Transforming growth factor (TGF)-β was originally identified in neoplastic cells and subsequently reported to be present in most cells in which it exerts a variety of effects on cell proliferation, cell differentiation, and embryogenesis. It has also been shown to stimulate the production of extracellular matrix components including collagens and fibronectin and to play a pivotal role in fibrogenesis (12). Thus, TGF-β is considered to be a mediator of collagen production in the models of fibrogenesis. Significant progress has recently been made in our understanding of the expression of the collagen genes and their transcriptional regulation by TGF-β (8, 9). A recent report has shown that high glucose transiently induces a transcriptional activity of c-*fos* responsible for stimulation of the TGF-β (13). However, there is little information regarding the interaction between AGE and c-*Fos*. We investigated here the expression of c-*Fos* in cultured mesangial cells treated with AGE and examined whether c-*Fos* affected the expression of TGF-β.

Furthermore, our recent report demonstrates that type IV collagen is up-regulated by AGE and its overexpression is transcriptionally regulated by Smad1 (14). Smad1 also enhances the levels of expression of type I collagen and osteopontin and plays a critical role in TGF-β-mediated overexpression of extracellular matrix in diabetic nephropathy (14). Therefore, we examined the role of Smad1 for regulating HSP47 expression by AGE stimulation in mesangial cells.

In this study, we reported on a study of the inhibitory effect of OPB-9195 (OPB), a novel inhibitor of AGEs formation, in a model of diabetic nephropathy. The pathogenic role of HSP47 in the development of the glomerulosclerotic lesions in diabetes was examined. We also confirmed the mechanism of these processes with the use of cultured mesangial cells.

* This work was supported in part by the "Research for the Future" Program for the Promotion of Science (Grant 97L00805). The costs of publication of this article were defrayed in part by the payment of page charges. This article must therefore be hereby marked "*advertisement*" in accordance with 18 U.S.C. Section 1734 solely to indicate this fact.

¶¶ To whom correspondence should be addressed: Dept. of Clinical Biology and Medicine, Course of Biological Medicine, School of Medicine, The University of Tokushima, 3-18-15 Kuramoto-cho, Tokushima 770-8503, Japan. Tel.: 81-88-633-7184; Fax: 81-88-633-9245; E-mail: doi@clin.med.tokushima-u.ac.jp.

[1] The abbreviations used are: AGEs, advanced glycation end-products; HSP47, 47-kDa heat shock protein; iNOS, inducible nitric-oxide synthase; OPB, OPB-9195; TGF, transforming growth factor; CML, carboxymethyllysine; BSA, bovine serum albumin; GAPDH, glyceraldehyde-3-phosphate dehydrogenase; siRNA, small interfering RNA.

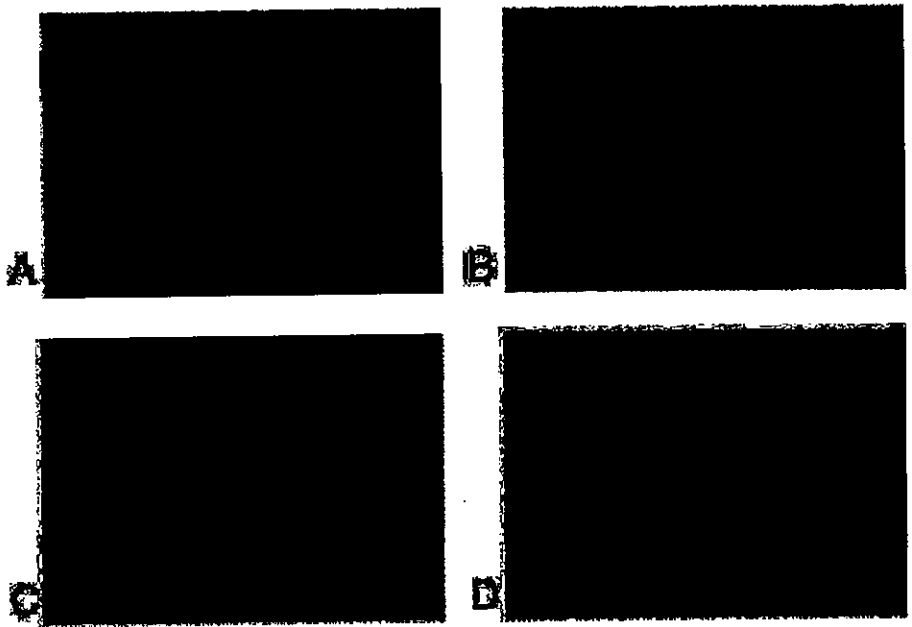

FIG. 1. **Light microscopy examination.** The microscopic lesions in iNOSTg mice took the form of diffuse proliferation of mesangial matrix and an expansion of the mesangial area. These lesions were ameliorated by treatment with OPB. *A*, control. *B*, iNOSTg. *C*, control + OPB. *D*, iNOSTg + OPB.

MATERIALS AND METHODS

Experimental Animals—iNOSTg were maintained on CD-1 mouse background (11). Male littermates were screened for the transgenes by the PCR amplification and used for analysis. The primers used for the detection of iNOSTg were as follows: forward primer, 5′-GTGGGCTA-TGGGTTTGTGGAAGGAGA-3′, and reverse primer 5′-CGATGTCACA-TGCAGCTTGT-3′.

No expression of iNOS protein, whose synthesis is directed only in pancreatic islets, was detected in the kidney. The mice were divided into four groups: CD-1 as control mice (Control); control mice treated with OPB (Control + OPB); iNOSTg; and iNOSTg treated with OPB (iNOSTg + OPB). Each group was fed either normal chow or the chow containing 0.28% OPB (provided by Fujii Memorial Research Institute, Otsuka Pharmaceutical, Tokushima, Japan) from 1 to 6 months after birth.

Blood Glucose and HbA1c Concentration—The levels of blood glucose and HbA1c were measured from the tail vein blood using Dexter Z sensor (Bayer-Medical, Tokyo, Japan) and DCA2000 analyzer (Bayer-Medical), respectively.

Determination of AGEs Concentration—Levels of serum carboxymethyllysine (CML) and non-CML AGEs were determined using a competitive enzyme-linked immunosorbent assay as described previously (15). 1 unit/ml CML or non-CML AGEs corresponded to a protein concentration of 1 μg/ml CML-bovine serum albumin (BSA) or non-CML AGE-BSA, respectively.

Renal Histology and Morphometric Analysis—Kidneys were processed for light microscopy examination, and the severity of the renal sclerosis was scored on an arbitrary scale from 0 to 4. The mean glomerular volume was determined as described previously (3, 16).

Immunofluorescence Analysis for HSP47, Types I and IV Collagens, and TGF-β—Immunofluorescence analysis was carried out as described previously using an affinity-purified polyclonal antibody specific to HSP47, types I and IV collagens, and TGF-β (8, 9).

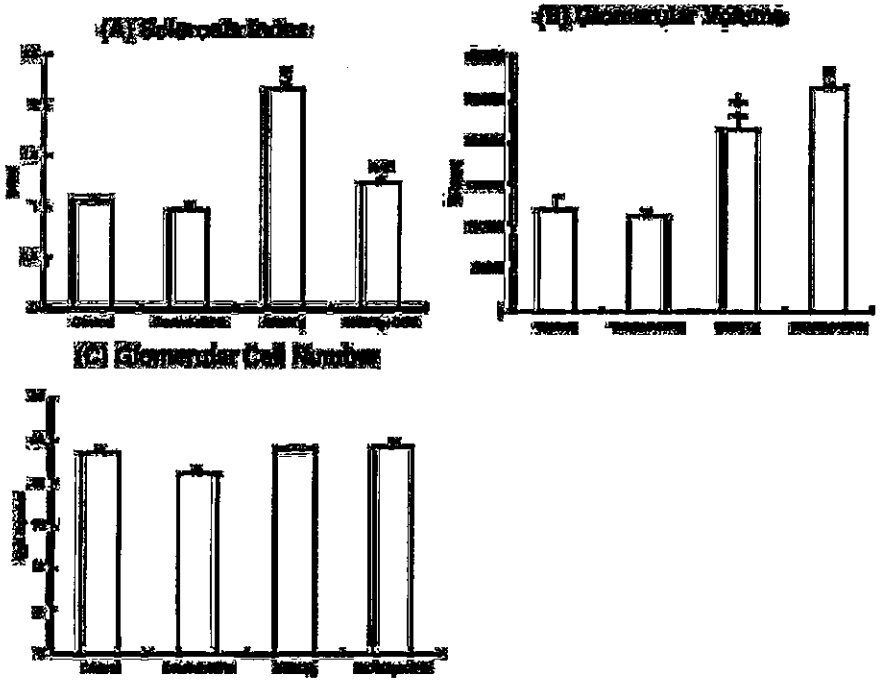

FIG. 2. **Effects of OPB in diabetic glomerulosclerosis.** OPB markedly improved glomerulosclerosis in iNOSTg mice (*A*) with no decrease in of glomerular volume (*B*). *C*, no significant differences in glomerular cell number were found. Number of experiments: Control, 11; OPB(−), 9; and OPB(+), 10. *, $p < 0.05$ *versus* Control; **, $p < 0.05$, OPB(+) *versus* OPB(−).

Laser-manipulated Microdissection and Laser Pressure Catapulating—Laser-manipulated microdissection is a method to cut out a small region from a specimen under microscope observation by means of laser beam. Laser pressure catapulating is a method to push up and collect samples that have been microdissected using laser-manipulated microdissection by means of a strong laser. These methods were performed using the Robot-Microbeam (P.A.L.M) and an inverted microscope (Carl Zeiss, Oberkochem, Germany) (17). By tracing around the glomeruli shown on the monitor, the targeted glomeruli were cut out by the laser. For laser pressure catapulating, the setting for the laser energy should be sufficiently high to catapult the microdissected glomeruli of the histologic specimen into the microcentrifuge cap, which was held in place by the micromanipulator. When the laser pressure catapulating was performed, the microdissected glomeruli "jumped up" and were attached to the cap. 60–80 glomeruli for each experiment were collected from this procedure. Glomeruli were obtained from those of control, iNOSTg, and iNOSTg-OPB mice at 24 weeks of age.

Quantitative PCR—Total RNA was prepared from isolated glomeruli, and a cDNA synthesis was performed with reverse transcription. Real-time PCR was performed by using the ABI Prism 7700 sequence detection system (PerkinElmer Life Sciences). Primers for mouse glyceraldehyde-3-phosphate dehydrogenase (*GAPDH*) (PerkinElmer Life Sciences) were used for internal control. The primers for HSP47, type IV collagen, and TGF-β were as follows: HSP47 (forward primer, 5′-GCGAGATAATCAGAGCGGCT-3′; reverse primer, 5′-CCACGCCCACTCTTGGACT-3′; and *Taq*Man Probe, 5′-CTTGCTCTTCATTGGCCGCCTGG-3′); type IV collagen (forward primer, 5′-GACCCCGAGGTTAGGAAGG-3′; reverse primer, 5′-CACTCGGTCCATGATCCCA-3′; and *Taq*Man Probe, 5′-ATCGAGCCGAGCCTAGAGCTGAAAGA-3′); and TGF-β (forward primer, 5′-AAGTCACCCGCGTGCTAATG-3′; reverse primer, 5′-CCCGAATGTCTGACGTATTGAA-3′; and *Taq*Man Probe, 5′-TGGACCGCAACAACGCAATCTATG-3′).

The cleavage of the sequence-specific probe (*Taq*Man Probe) by 5′-nuclease activity of the *Taq*DNA polymerase releases the reporter dye, resulting in an emission increase. With each cycle, the fluorescence intensity of additional reporter dye molecules is monitored by the system. The threshold cycles were selected in the line in which all of the samples were in the logarithmic phase. The quantity of PCR products was calculated from the threshold cycle value. This real-time detection generates quantitative data based on PCR at early cycles when PCR fidelity is highest (18, 19).

Cell Culture—A glomerular mesangial cell line was established from glomeruli isolated from normal 4-week-old mice (C57BL/6JxSJLJ) and was identified according to a method described previously (4, 5). The mesangial cells were plated on 100-mm plastic dishes (Nunc) that were maintained in B medium (a 3:1 mixture of minimal essential medium/F12 modified with trace elements) supplemented with 1 mM glutamine, penicillin at 100 units/ml, streptomycin at 100 μg/ml, and 20% fetal calf serum (Irvine Scientific). The cells were passaged weekly with trypsin-EDTA. The cultured cells fulfilled the previously described criteria generally accepted for glomerular mesangial cells (20).

AGE-BSA—AGE-BSA was prepared by the method described previously (5, 21). BSA was incubated with glucose 6-phosphate for >60 days at 37 °C. AGE content was measured by the fluorescence intensity at a protein concentration of 1 mg/ml. Control BSA was prepared by incubating BSA without glucose 6-phosphate under the same conditions as those for AGE-BSA. AGE-BSA and control BSA contained 61.3 and 8.31 AGE units/mg protein, respectively. Protein concentrations were determined by the method of Bradford using BSA as the standard.

Mesangial cells were plated in the B medium, 20% fetal bovine serum at 5×10^5/well in six-well dishes, that had been coated with AGE-BSA or control BSA at 50 μg/cm² for 72 h. After the treatment, the cells were washed with phosphate-buffered saline and total RNA was isolated using TRIzol reagent (Invitrogen).

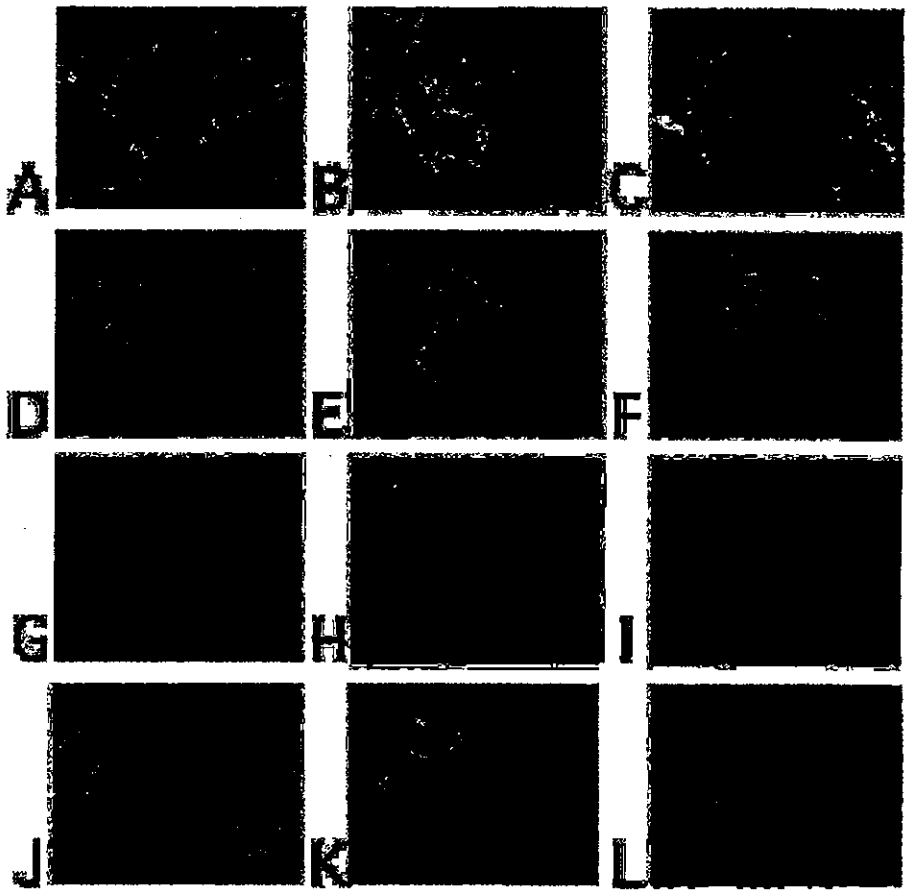

FIG. 3. **Immunofluorescence analysis of HSP47, collagens, and TGF-β.** A remarkable increase in the expression of HSP47, types I and IV collagens, and TGF-β was seen. OPB treatment led to show a significant decrease. *A–C*, type I collagen; *D–F*, type IV collagen. *G–I*, HSP47. *J–L*, TGF-β. *A*, *D*, *G*, and *J*, control. *B*, *E*, *H*, and *K*, iNOSTg. *C*, *F*, *I*, and *L*, iNOSTg + OPB.

TGF-β-neutralizing Antibody Assay—The cells were resuspended at a concentration of 1×10^6 cells/ml and plated onto 100-mm dish either in the presence of 10 μg/ml TGF-β1-neutralizing antibody (R&D Systems) or a control normal IgG (22). After 24 h of incubation, the cells were harvested and underwent RNA isolation on real-time reverse transcription-PCR.

Smad1 Morpholino Antisense Oligonucleotide—The antisense oligonucleotide for *Smad1* was a 25-nucleotide morpholino oligomer (Genetools LLC) with the base composition of 5′-CAAGCTGGTCACATTCATAGCGGCT-3′. A standard morpholino oligomer with the base composition of 5′-CAtGCTcGTCACATTCAaAGCcGCT-3′ (points of mismatch are shown by *small letters*) was used as a control. Microinjection of *in vitro* transcribed RNA was performed as described previously (14).

Western Blotting—Cultured mesangial cells were harvested in sample buffer, resolved by SDS-polyacrylamide gel electrophoresis, transferred to nitrocellulose membrane, subjected to Western blot using a 1:500 dilution of antibody for HSP47, type IV collagen, and TGF-β (8, 9), and detected using an enhanced chemiluminescence detection system (Invitrogen).

RNase Protection Assay—Total RNA was isolated from mesangial cells using the TRIzol reagent, and an RNase protection assay was performed as described previously (14, 22). The RNA probes were prepared by linearizing the PvuII fragment of type IV collagen from p1234, the SacI fragment of *Smad1* from pGEM-T, and the EcoRI fragment of *GAPDH* from pMGAP1. In addition, mouse riboprobe for HSP47 (5′-TCCTATACTGTGGGTGTTACGATGA-3′ and 5′-TACAACTCATCTCGCATCTTGTCTC-3′), *c-fos* (5′-TATCTCCTGAAGAGGAAGAGAAACG-3′ and 5′-AACAAGAAGTCATCAAAGGGTTCTG-3′), and TGF-β (5′-ATACCAACTATTGCTTCAGCTCCAC-3′ and 5′CACGTAGTAGACGATGGGCAGT-3′) was amplified by reverse transcription-PCR. The PCR fragments were sequenced to confirm to be cDNAs, respectively, and

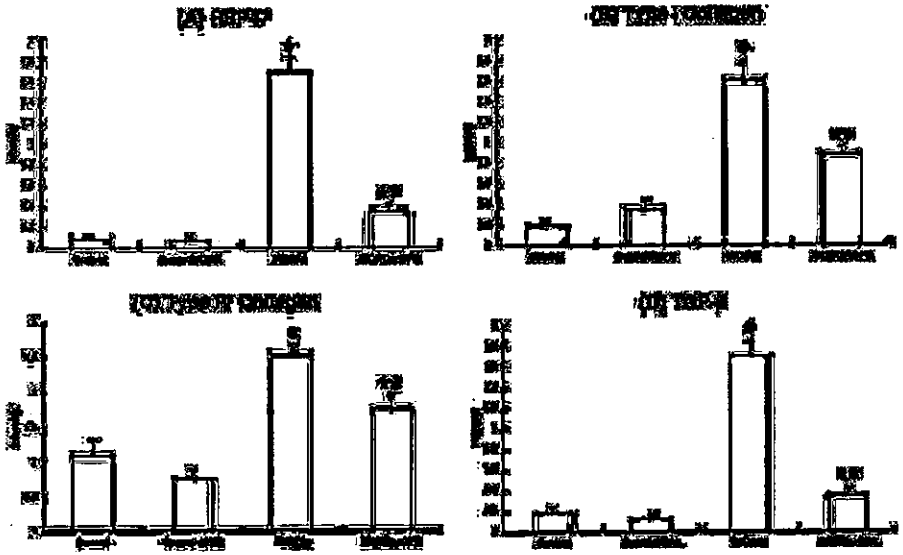

FIG. 4. **Arbitrary scaling of expressions of HSP47, collagens, and TGF-β.** A remarkable increase in the expression of HSP47 (*A*), types I (*B*) and IV (*C*) collagens, and TGF-β (*D*) was seen. OPB treatment showed a significant decrease. *, $p < 0.05$; *versus* Control; **, $p < 0.05$, OPB(+) *versus* OPB(−).

were cloned into a pGEM-T plasmid. After digesting the plasmid with SacI, an antisense riboprobe was synthesized *in vitro* using T7 RNA polymerase. The RNA probes and the test RNA were hybridized overnight at 45 °C. RNase A (40 μg/ml) and RNase T1 (2 μg/ml) were added to each tube, and the tubes were incubated for 1 h at 30 °C. The RNase resistant fragments were analyzed by 5% polyacrylamide, 8 M urea gel electrophoresis. The protected bands for each RNA probe had the same size as the coding sequence for the specific mRNA.

Small Interfering RNA (siRNA) and Transfections—The siRNA sequence targeting *c-fos* (5′-CCAATCTGCTGAAGAGAAGGAAAA-3′) was purchased from Hokkaido Science (Sapporo, Japan). Cells were transfected with LipofectAMINE 2000 (Invitrogen) according to the manufacturer's protocol in the presence of siRNA. siRNA against *Luciferase GL2* (5′-CGTACGCGGAATACTTCGA-3′) (Dharmacon) was used as a control.

RESULTS

Blood Glucose, HbA1c, and AGE Concentration—Blood glucose levels of iNOSTg mice were >500 mg/dl (503 ± 19 mg/dl, $n = 9$), and OPB had no effect on this parameter (586 ± 74 mg/dl, $n = 5$). HbA1c levels were over 7% in iNOSTg mice (7.5 ± 0.8%), whereas that of controls was below the detection limit. Both serum levels of CML and non-CML AGEs were significantly higher in iNOSTg mice (7.3 ± 0.6 and 20.7 ± 2.5 units/ml, respectively) than controls (6.2 ± 0.4 and 12.6 ± 1.0 units/ml, respectively), whereas OPB treatment of iNOSTg mice led to a decrease to the control levels (4.3 ± 1.0 and 10.2 ± 2.6 units/ml, respectively).

Response of Matrix Expansion to Treatment with OPB—The microscopic lesions in iNOSTg mice were observed as a diffuse proliferation of the mesangial matrix and the expansion of the mesangial area (Fig. 1). These lesions were ameliorated by treatment with OPB. OPB markedly improved the glomerulosclerosis of iNOSTg mice with no decrease in glomerular volume. No significant differences in glomerular cell number were detected among these groups (Fig. 2).

Response of Expressions of Collagens and HSP47 to Treatment with OPB—Although only traces of type I collagen could be detected in control glomeruli, it was strongly expressed in the mesangial area of glomeruli in iNOSTg mice. OPB treatment decreased this expression. Type IV collagen was expressed in both the glomerular basement membrane and the mesangium in control mice. Mesangial expression was increased in iNOSTg mice, which decreased after treatment with OPB. Immunofluorescent staining also revealed a remarkable increase in the expression of HSP47, which paralleled the expression of type I and type IV collagen and TGF-β in iNOSTg mice. These expressions were decreased as the result of OPB treatment (Figs. 3 and 4).

Quantitation of the Expression Ratio of HSP47/GAPDH mRNA and Type IV Collagen/GAPDH mRNA in Glomeruli by Real-time RT-PCR—Isolated mRNA of 50 glomeruli randomly selected from 5-μm frozen sections by laser-manipulated microdissection and laser pressure catapulating was used to quantitate the expression of HSP47 and type IV collagen mRNA in this diabetic nephropathy model. A remarkable increase in the expression of HSP47, type IV collagen, and TFG-β was seen in iNOSTg mice, and OPB treatment showed a significant decrease (Fig. 5).

Stimulation by AGEs in Cultured Mesangial Cells—To confirm the mechanism, cultured mesangial cells were stimulated with AGEs. AGEs significantly increased both HSP47 and type IV collagen expressions. In addition, AGEs were found to enhance the expression of TGF-β in cultured mesangial cells (Fig. 6*a*). Similarly, the levels of both HSP47 and type IV collagen proteins increased in accordance with the elevation of TGF-β protein (Fig. 6*b*). Neutralizing antibody for TGF-β inhibited overexpression of both HSP47 and type IV collagen (Fig. 7, *a* and *b*).

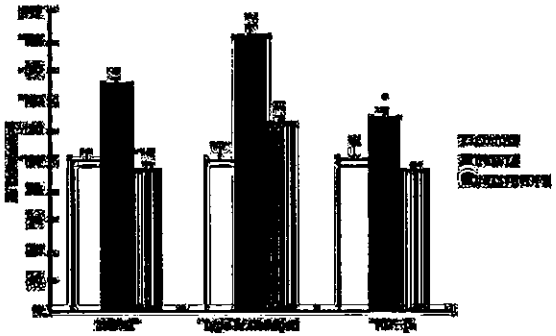

FIG. 5. **Glomerular mRNA expression.** Number of experiments: Control, 4; OPB(−), 5; and OPB(+), 6. *, $p < 0.05$ *versus* Control; **, $p < 0.05$, OPB(+) *versus* OPB(−).

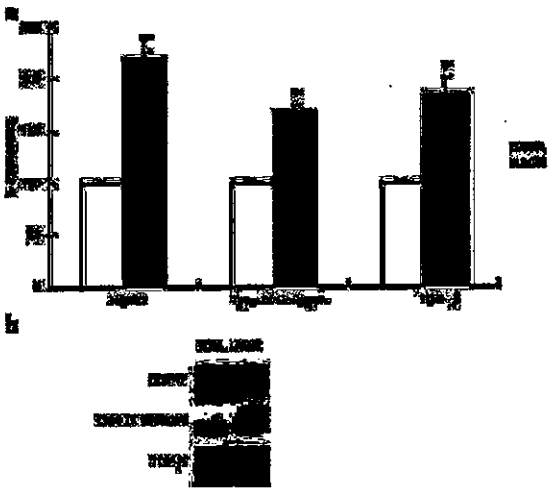

FIG. 6. **Effects of AGE in cultured mesangial cells.** *a*, AGE stimulation increased mRNA expressions of HSP47, TGF-β, and type IV collagen in cultured mesangial cells (number of experiments, 5). *, $p < 0.05$ *versus* Control (BSA). *b*, HSP47, type IV collagen, and TGF-β were monitored by Western blot in response to a 72-h treatment with AGE or BSA. One of three independent experiment is shown.

To further elucidate the mechanism for AGE-mediated induction of TGF-β, we investigated the expression of c-*fos* in mesangial cells. We found that AGE treatment caused a significant increase of *c-fos* mRNA by RNase protection assay. The AGE-mediated induction of *c-fos* was completely abolished in the presence of the specific siRNA but not in the presence of control siRNA. Consistent with the inhibition of *c-fos*, the induction of TGF-β was strongly attenuated (Fig. 8).

We next examined the involvement of Smad1 in TGF-β-mediated induction of HSP47 and type IV collagen expression. We transfected antisense morpholino oligomers to block Smad1-mediated effect in mesangial cells. Mesangial cells transfected with Smad1-antisense oligomers showed much less expression of HSP47 and type IV collagen transcripts after AGE stimulation than those with control oligomers (Fig. 9).

DISCUSSION

This study shows that the collagen-specific chaperone protein, HSP47, is strongly expressed in glomerulosclerotic lesions in parallel with increased expression of collagens I and IV in diabetic nephropathy. The findings of the study also suggest that AGEs are a key factor in the synthesis of increased expression of both HSP47 and collagens *in vitro* and *in vivo*. Our *in vitro* study indicates that AGEs-mediated induction of HSP47 and collagens may be through TGF-β.

Collagen is synthesized in the form of pro-α chains, and three pro-α chains form procollagen with a triple-helical structure in the endoplasmic reticulum. HSP47 is a collagen-binding stress protein and has been shown to be localized exclusively in the endoplasmic reticulum. Procollagen polypeptides form a complex with HSP47 in the endoplasmic reticulum, which plays an important role as a collagen-specific molecular chaperone in the intracellular processing/folding of procollagen molecules (23, 24). The crucial role of HSP47 in regulating biosynthesis of collagen molecules has been reported previously (25), and transcriptional regulation for HSP47 expression was clarified (26, 27). However, its role in kidney diseases in relation to sclerosis/fibrosis in diabetic nephropathy and IgA nephropathy is completely unknown. We and others (8, 28) have demonstrated that HSP47 in glomerulosclerosis is associated with collagen staining. Furthermore, the blocking of HSP47 with antisense

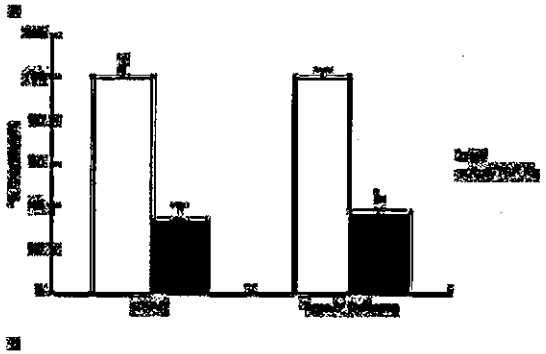

FIG. 7. **Inhibition of HSP47 and type IV collagen by TGF-β-neutralizing antibody.** *a*, neutralizing antibody for TGF-β inhibited both HSP47 and type IV collagen mRNA expressions in cultured mesangial cells (number of experiments, 5; *, $p < 0.05$ *versus* Control (IgY)). *b*, Western blot analysis of HSP47 and type IV collagen protein expression in cultured mesangial cells treated with AGE in the presence of neutralizing antibody for TGF-β or control (IgY).

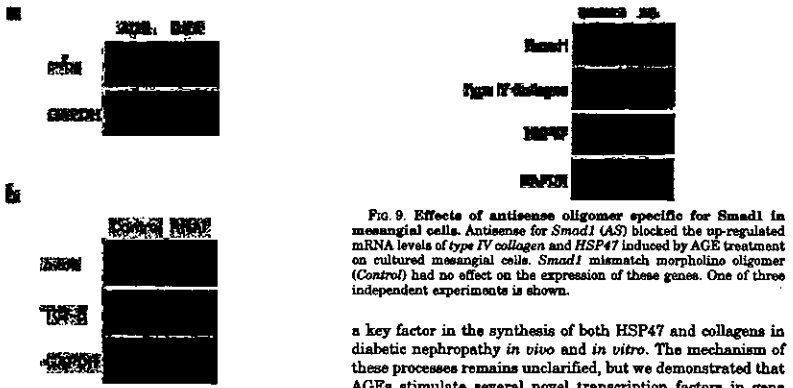

FIG. 8. **Regulation of *c-fos* mRNA expression by AGE.** *a*, RNase protection assay analysis of *c-fos* mRNA expression in total RNA lysates from cultured mesangial cells treated with AGE. One of three independent experiments is shown. *GAPDH* was used as an internal control. *b*, RNA interference (*RNAi*) against *c-fos* blocked the up-regulated mRNA level of *TGF-β* induced by AGE treatment. One of three independent experiments is shown.

FIG. 9. **Effects of antisense oligomer specific for Smad1 in mesangial cells.** Antisense for *Smad1* (*AS*) blocked the up-regulated mRNA levels of *type IV collagen* and *HSP47* induced by AGE treatment on cultured mesangial cells. *Smad1* mismatch morpholino oligomer (*Control*) had no effect on the expression of these genes. One of three independent experiments is shown.

oligonucleotides caused a dramatic amelioration of glomerular lesions in the rat glomerulonephritis model (9). These findings suggest that HSP47 is a key factor in the development of various glomerular injuries. In this study, a close relationship of HSP47 to glomerulosclerosis in diabetic nephropathy was found.

The blocking of AGEs formation inhibited the overreproduction of HSP47 and collagens, thereby suppressing the gene expression of type IV collagen, extracellular matrix accumulation, and glomerulosclerosis in diabetic nephropathy *in vivo*. AGEs also increased mRNA expression of both HSP47 and type IV collagen *in vitro*. Thus, our study implicates that AGEs are a key factor in the synthesis of both HSP47 and collagens in diabetic nephropathy *in vivo* and *in vitro*. The mechanism of these processes remains unclarified, but we demonstrated that AGEs stimulate several novel transcription factors in gene expression for glomerulosclerosis (5). We have recently reported that Smad1 transcriptionally regulates of type IV collagen under AGE stimulation (14). Here, we also observed that the expression of HSP47 was regulated by Smad1 under AGE exposure. Yamamura *et al.* (29) has reported that TGF-β transcriptionally activates *HSP47* gene expression. Thus, Smad1 may partially participate in the TGF-β-mediated up-regulation of HSP47.

It has been shown that TGF-β stimulates the production of extracellular matrix components including collagens and fibronectin and that it plays a key role in glomerulosclerosis (12). TGF-β regulates the expression of the collagen genes and their transcriptional activities. In particular, the promoter analysis of the collagen genes revealed that TGF-β1 regulates the transcription of collagen genes via several *cis*-elements of their promoters (13). TGF-β also increases HSP47 gene expression in other cell types (29). We first demonstrated that TGF-β stimulates not only collagen but also HSP47 in mesangial cells. In addition, we showed that c-*Fos* participates in the induction of TGF-β under AGE exposure. These data suggest that TGF-β and its signaling pathway are important targets for treating diabetic nephropathy.

Most experimental models of diabetic nephropathy are different from human pathological lesions (10, 30). On the other hand, the iNOSTg mice showed remarkably advanced glomerular lesions that resemble human diabetic glomerulosclerosis. From the analysis of this model, we confirmed that glomerular hypertrophy is important in the development of diabetic nephropathy because the iNOSTg mice showed glomerular hypertrophy in association with typical glomerulosclerosis. However, the intervention of AGE formation showed a decreased level of glomerulosclerosis with no evidence for diminished glomerular hypertrophy. The mechanism for this is unclear, but the regulation of HSP47 and collagens seemed to be independent of the control of glomerular hemodynamics. Further investigation will be needed to clarify the mechanism of these findings.

REFERENCES

1. Bojestig, M., Arnqvist, H. J., Hermansson, G., Karlberg, B. E., and Ludvigsson, J. (1994) *N. Engl. J. Med.* **330**, 15–18
2. Vlassara, H., Bucala, R., and Striker, L. (1994) *Lab. Investig.* **70**, 138–151
3. Yamamoto, Y., Kato, I., Doi, T., Yonekura, H., Ohashi, S., Takeuchi, M., Watanabe, T., Yamagishi, S., Sakurai, S., Takasawa, S., Okamoto, H., and Yamamoto, H. (2001) *J. Clin. Investig.* **108**, 261–268
4. Doi, T., Vlassara, H., Kirstein, M., Yamada, Y., Striker, G. E., and Striker, L. J. (1992) *Proc. Natl. Acad. Sci. U. S. A.* **89**, 2873–2877
5. Ishara, N., Takeoka, H., Yamada, Y., Kita, T., and Doi, T. (1998) *Kidney Int.* **50**, 1166–1172
6. Soulis-Liparota, T., Cooper, M., Papazoglou, D., Clarke, B., and Jerums, G. (1991) *Diabetes* **40**, 1328–1334
7. Nakamora, S., Makita, Z., Ishikawa, S., Yamamura, K., Fujii, W., Yanagisawa, K., Kawata, T., and Koike, T. (1997) *Diabetes* **46**, 895–899
8. Sunamoto, M., Kuze, K., Ishara, N., Takeoka, H., Nagata, K., Kita, T., and Doi, T. (1998) *Int. J. Exp. Pathol.* **79**, 133–140
9. Sunamoto, M., Kuze, K., Tsuji, H., Ohishi, N., Yagi, K., Negata, K., Kita, T., and Doi, T. (1998) *Lab. Investig.* **78**, 967–972
10. Doi, T., Hattori, M., Agodoa, L. Y., Sato, T., Yoshida, H., Striker, L. J., and Striker, G. E. (1990) *Lab. Investig.* **63**, 204–212
11. Takamura, T., Kato, I., Kimura, N., Nakazawa, T., Yonekura, H., Takasawa, S., and Okamoto, H. (1998) *J. Biol. Chem.* **273**, 2493–2496
12. Border, W. A., and Ruoslahti, E. (1992) *J. Clin. Investig.* **90**, 1–7
13. Weigert, C., Brodbeck, K., Bierhaus, A., Haring, H. U., and Schleicher, E. D. (2003) *Biochem. Biophys. Res. Commun.* **304**, 301–307
14. Abe, H., Matsubara, T., Iehara, N., Nagai, K., Takahashi, T., Arai, H., Kita, T., and Doi, T. (2004) *J. Biol. Chem.* **279**, 14201–14206
15. Takeuchi, M., Makita, Z., Yanagisawa, K., Kameda, Y., and Koike, T. (1999) *Mol. Med.* **5**, 393–405
16. Doi, T., Striker, L. J., Gibson, C. C., Agodoa, L. Y., Brinster, R. L., and Striker, G. E. (1990) *Am. J. Pathol.* **137**, 541–552
17. Schutze, K., and Lahr, G. (1998) *Nat. Biotechnol.* **16**, 737–742
18. Fink, L., Seeger, W., Ermert, L., Hanze, J., Stahl, U., Grimminger, F., Kummer, W., and Bohle, R. M. (1998) *Nat. Med.* **4**, 1329–1333
19. Makibayashi, K., Tatematsu, M., Hirata, M., Fukushima, N., Kusano, K., Ohashi, S., Abe, H., Kuze, K., Fukatsu, A., Kita, T., and Doi, T. (2001) *Am. J. Pathol.* **158**, 1733–1741
20. MacKay, K., Striker, L. J., Elliot, S., Pinkert, C. A., Brinster, R. L., and Striker, G. E. (1988) *Kidney Int.* **33**, 677–684
21. Tsuji, H., Ishara, N., Masegi, T., Izoura, M., Ohkawa, J., Arai, H., Ishii, K., Kita, T., and Doi, T. (1998) *Biochem. Biophys. Res. Commun.* **245**, 583–588
22. Abe, H., Ishara, N., Utsumomiya, K., Kita, T., and Doi, T. (1999) *J. Biol. Chem.* **274**, 20674–20678
23. Nagata, K., Saga, S., and Yamada, K. M. (1988) *Biochem. Biophys. Res. Commun.* **153**, 428–434
24. Nakai, A., Satoh, M., Hirayoshi, K., and Nagata, K. (1992) *J. Cell Biol.* **117**, 903–914
25. Nagai, N., Hosokawa, M., Itohara, S., Adachi, E., Matsushita, T., Hosokawa, N., and Nagata, K. (2000) *J. Cell Biol.* **150**, 1499–1506
26. Hirata, H., Yamamura, I., Yasuda, K., Kobayashi, A., Tada, N., Suzuki, M., Hirayoshi, K., Hosokawa, N., and Nagata, K. (1999) *J. Biol. Chem.* **274**, 35703–35710
27. Yasuda, K., Hirayoshi, K., Hirata, H., Kubota, H., Hosokawa, N., and Nagata, K. (2002) *J. Biol. Chem.* **277**, 44613–44622
28. Razzaque, M. S., Kumatori, A., Harada, T., and Taguchi, T. (1998) *Nephron* **80**, 434–443
29. Yamamura, I., Hirata, H., Hosokawa, N., and Nagata, K. (1998) *Biochem. Biophys. Res. Commun.* **244**, 68–74
30. Velasquez, M. T., Kimmel, P. L., and Michaelis, O. E., IV (1990) *FASEB J.* **4**, 2850–2859

Roles of thromboxane A_2 and prostacyclin in the development of atherosclerosis in apoE-deficient mice

Takuya Kobayashi,[1] Yoshio Tahara,[1] Mayumi Matsumoto,[1] Masako Iguchi,[1] Hideto Sano,[2] Toshinori Murayama,[3] Hidenori Arai,[2] Hiroji Oida,[4] Takami Yurugi-Kobayashi,[5] Jun K. Yamashita,[6] Hiroyuki Katagiri,[6,7] Masataka Majima,[7] Masayuki Yokode,[3] Toru Kita,[8] and Shuh Narumiya[1]

[1]Department of Pharmacology, [2]Department of Geriatric Medicine, and [3]Department of Clinical Innovative Medicine, Kyoto University Faculty of Medicine, Kyoto, Japan. [4]Fukui Safety Research Institute, Ono Pharmaceutical Co., Fukui, Japan. [5]Laboratory of Stem Cell Differentiation, Kyoto University Faculty of Medicine, Kyoto, Japan. [6]Department of Surgery and [7]Department of Pharmacology, Kitasato University School of Medicine, Kanagawa, Japan. [8]Department of Cardiovascular Medicine, Kyoto University Faculty of Medicine, Kyoto, Japan.

Production of thromboxane (TX) A_2 and PG I_2/prostacyclin (PGI_2) is increased in patients with atherosclerosis. However, their roles in atherogenesis have not been critically defined. To examine this issue, we cross-bred atherosclerosis-prone apoE-deficient mice with mice deficient in either the TXA receptor (TP) or the PGI receptor (IP). Although they showed levels of serum cholesterol and triglyceride similar to those of apoE-deficient mice, *apoE*$^{-/-}$*TP*$^{-/-}$ mice exhibited a significant delay in atherogenesis, and *apoE*$^{-/-}$*IP*$^{-/-}$ mice exhibited a significant acceleration in atherogenesis compared with mice deficient in apoE alone. The plaques in *apoE*$^{-/-}$*IP*$^{-/-}$ mice showed partial endothelial disruption and exhibited enhanced expression of ICAM-1 and decreased expression of platelet endothelial cell adhesion molecule 1 (PECAM-1) in the overlying endothelial cells compared with those of *apoE*$^{-/-}$*TP*$^{-/-}$ mice. Platelet activation with thrombin ex vivo revealed higher and lower sensitivity for surface P-selectin expression in platelets of *apoE*$^{-/-}$*IP*$^{-/-}$ and *apoE*$^{-/-}$*TP*$^{-/-}$ mice, respectively, than in those of *apoE*$^{-/-}$ mice. Intravital microscopy of the common carotid artery revealed a significantly greater number of leukocytes rolling on the vessel walls in *apoE*$^{-/-}$*IP*$^{-/-}$ mice than in either *apoE*$^{-/-}$*TP*$^{-/-}$ or *apoE*$^{-/-}$ mice. We conclude that TXA_2 promotes and PGI_2 prevents the initiation and progression of atherogenesis through control of platelet activation and leukocyte-endothelial cell interaction.

Introduction

It is now understood that atherosclerosis is an inflammation in the intima of large arteries that is triggered by high serum cholesterol and in which various types of cells including monocytes/macrophages, endothelial cells (ECs), smooth muscle cells (SMCs), T cells, and blood platelets exert a complex array of interaction (1). A variety of substances including cytokines, chemokines, and growth factors are suggested to induce, amplify, and modify this inflammatory process. One group of these mediators is prostanoids, which are produced from arachidonic acid by the action of COX and include various types of PGs and thromboxane (TX). Involvement of prostanoids in acute inflammation has been well documented based on the finding that aspirin-like NSAIDs are specific COX inhibitors. Among prostanoids, PG I_2/prostacyclin (PGI_2) and TXA_2 have attracted particular attention for their importance in cardiovascular diseases: the former, generated by vascular ECs, is a potent platelet inhibitor and vasodilator, and the latter, released from activated platelets, is a potent vasoconstrictor and platelet-aggregating agent. Indeed, low-dose aspirin that preferentially inhibits platelet-derived TXA_2 over endothelium-derived PGI_2 has been used as anti-platelet therapy for the prevention of myocardial infarction and recurrence of strokes. Although biosynthesis of PGI_2 and TXA_2 is increased in patients with atherosclerosis (2, 3), the roles of these molecules in the initiation and progression of atherosclerosis have not yet been critically examined.

The role played by prostanoids in atherogenesis has been studied mostly by examining the effects of various drugs in mice deficient in either apoE (*apoE*$^{-/-}$ mice) (4, 5) or the LDL receptor (LDLR) (*LDLR*$^{-/-}$ mice) (6). One group of such pharmacological studies has used low doses of aspirin in atherosclerotic model animals to evaluate the contribution of TXA_2. Cyrus et al. (7) fed *LDLR*$^{-/-}$ mice a high-fat diet, treated the mice with low-dose aspirin, and found that this dose of aspirin significantly retarded the development of atherosclerotic lesions, with a 64% reduction in an en face analysis and 29% in a cross-sectional analysis. In contrast, Cayatte et al. (8) used aspirin in *apoE*$^{-/-}$ mice and did not find retardation in the development of atherosclerotic lesions. This discrepancy could be attributed to the higher dose of aspirin used in the latter study, which may have inhibited prostanoid production in cells other than platelets, particularly PGI_2 in blood vessels. In the same study, Cayatte et al. (8) administered a TXA receptor (TP) antagonist, S-18886, to *apoE*$^{-/-}$ mice. They reported that administration of this drug indeed suppressed the extent of atherogenesis, but only marginally, by 21%. The other group of pharmacological studies has used isoform-specific COX inhibitors and has evaluated the roles of prostanoids in atherogenesis. COX exists as two isoforms encoded by two distinct genes (9): COX-1 is constitutively expressed in most tissues and mediates basal physiological functions, while COX-2 is induced by various types of stimuli and works "on demand" in such conditions as inflammation. There is now substantial evidence that the majority of PGI_2 is produced by COX-2 in vascular ECs, whereas production of TXA_2 by platelets is catalyzed by COX-1 (10). The COX-2–catalyzed PGI_2 production probably reflects induction of COX-2 by hemodynamic shear stress in the vasculature (11). The issue of whether COX-2–derived PGI_2 exerts any protective effect on atherosclerosis is important, given that many juvenile patients with arthritis are treated with selective COX-2 inhibitors (12) and a large-scale study (VIGOR) indicated an increased tendency for cardiovascular accidents associated with the use of such drugs versus the nonselective COX inhibitor naproxen (discussed in ref. 13). Experiments examining the effects of COX-2 inhibitors in atherogenesis have yielded conflicting results. One study in which an MF-tricyclic was administered to *apoE*$^{-/-}$ mice found exaggeration of atherosclerosis (14), and one study examining the effect of rofecoxib in *LDLR*$^{-/-}$ mice detected a small but significant suppression in the development of atherosclerosis (15). The former study (14) did not specify the gender of the mice studied and may be difficult to interpret. However, two other studies, one of nimesulide in *LDLR*$^{-/-}$ mice (16) and the other of SC-236 in *apoE*$^{-/-}$ mice (17), did not find significant effects. These studies, except for the study using MF-tricyclic (14), all detected similar suppression of PGI_2 production in animals given these drugs. However, the suppression remained partial,

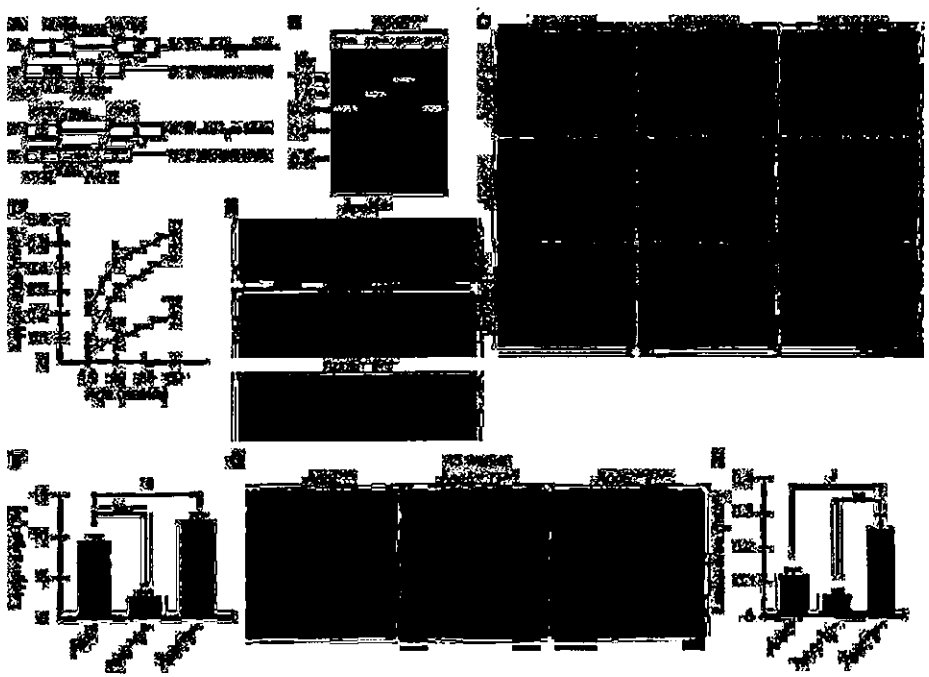

Figure 1
Generation and atherosclerotic lesions of *apoE*$^{+/-}$*TP*$^{-/-}$ and *apoE*$^{+/-}$*IP*$^{+/-}$ mice. (A) Strategy for PCR analysis of WT and targeted alleles of TP and IP. Primers are shown by arrowheads. Amplified fragments are shown by broken lines. Neo, neomycin-resistance gene. (B) Representative PCR for TP and IP alleles of *apoE*$^{+/+}$, *apoE*$^{+/-}$*TP*$^{+/+}$, and *apoE*$^{+/-}$*IP*$^{+/+}$ mice. (C) Representative oil red O staining of aortic sinus sections of *apoE*$^{+/+}$ (middle), *apoE*$^{+/-}$*TP*$^{+/+}$ (lower), and *apoE*$^{+/-}$*IP*$^{+/+}$ (upper) mice. Scale bar: 200 μm. (D) Time course of atherosclerotic lesion development in *apoE*$^{+/+}$ (open circles), *apoE*$^{+/-}$*TP*$^{+/+}$ (filled circles), and *apoE*$^{+/-}$*IP*$^{+/+}$ (filled squares) mice. Data are means ± SEM (n = 10 for 15-week-old *apoE*$^{+/+}$ and *apoE*$^{+/-}$*IP*$^{+/+}$ and 20-week-old *apoE*$^{+/+}$ and *apoE*$^{+/-}$*TP*$^{+/+}$ male mice; n = 6 for 15-week-old *apoE*$^{+/-}$*TP*$^{+/+}$, 20-week-old *apoE*$^{+/-}$*IP*$^{+/+}$, and 30-week-old *apoE*$^{+/+}$, *apoE*$^{+/-}$*TP*$^{+/+}$, and *apoE*$^{+/-}$*IP*$^{+/+}$ mice). *P < 0.05 and **P < 0.01 versus *apoE*$^{+/+}$ mice. (E) Representative Sudan IV staining of en face preparations of aortas from *apoE*$^{+/+}$, *apoE*$^{+/-}$*TP*$^{+/+}$, and *apoE*$^{+/-}$*IP*$^{+/+}$ mice at 20 weeks of age. Scale bars: 2 mm. (F) Quantification of en face atherosclerotic lesions in *apoE*$^{+/+}$, *apoE*$^{+/-}$*TP*$^{+/+}$ and *apoE*$^{+/-}$*IP*$^{+/+}$ mice at 20 weeks of age. Data are means ± SEM (n = 5 each). *P < 0.05 and **P < 0.01 for bracketed comparisons. (G) Representative hematoxylin and eosin staining of innominate artery sections of *apoE*$^{+/+}$, *apoE*$^{+/-}$*TP*$^{+/+}$, and *apoE*$^{+/-}$*IP*$^{+/+}$ mice at 45 weeks of age. Scale bar: 20 μm. (H) Quantitative analysis of innominate atherosclerotic areas in *apoE*$^{+/+}$, *apoE*$^{+/-}$*TP*$^{+/+}$, and *apoE*$^{+/-}$*IP*$^{+/+}$ mice at 45 weeks of age. Data are means ± SEM (n = 10 each). *P < 0.05 and **P < 0.01 for bracketed comparisons.

Nonstandard abbreviations used: EC, endothelial cell; HDLC, HDL-cholesterol; IP, PGI receptor; LDLC, LDL-cholesterol; LDLR, LDL receptor; PECAM-1, platelet endothelial cell adhesion molecule 1; PFA, paraformaldehyde; PGI_2, PG I_2/prostacyclin; PRP, platelet-rich plasma; SMC, smooth muscle cell; TC, total cholesterol; TG, total triglyceride; TP, TXA receptor; TX, thromboxane; VLDLC, VLDL-cholesterol; vWF, von Willebrand factor.

Conflict of interest: The authors have declared that no conflict of interest exists.

Citation for this article: *J. Clin. Invest.* 114:784–794 (2004). doi:10.1172/JCI200421446.

Table 1
Plasma cholesterol and triglyceride levels

Mouse (mg/dl)	TC (mg/dl)	TG (mg/dl)	VLDLC (mg/dl)	LDLC (mg/dl)	HDLC
C57BL/6 ($n = 8$)	99 ± 5	57 ± 4	6 ± 1	24 ± 3	58 ± 4
$TP^{-/-}$ ($n = 8$)	85 ± 9	50 ± 5	8 ± 1	19 ± 3	54 ± 4
$IP^{-/-}$ ($n = 8$)	90 ± 9	55 ± 6	7 ± 1	22 ± 3	56 ± 4
$ApoE^{-/-}$ ($n = 8$)	535 ± 43[A]	102 ± 6[A]	381 ± 36[A]	127 ± 5[A]	27 ± 4[B]
$ApoE^{-/-}TP^{-/-}$ ($n = 8$)	595 ± 53[A]	105 ± 10[A]	395 ± 60[A]	138 ± 5[A]	22 ± 4[B]
$ApoE^{-/-}IP^{-/-}$ ($n = 8$)	588 ± 52[A]	103 ± 8[A]	430 ± 44[A]	135 ± 11[A]	22 ± 4[B]

All data are shown as mean ± SEM. [A]$P < 0.01$ versus C57BL/6. [B]$P < 0.05$ versus C57BL/6.

supporting a view that both COX-1 and COX-2 contribute to PGI_2 production under pathological conditions such as atherosclerosis (3). Thus, pharmacological approaches using various drugs have produced variable and inconclusive results and have failed to provide a cohesive picture on the contribution of prostanoids, including PGI_2 and TXA_2, to atherogenesis. This probably reflects the inherent limitations associated with pharmacological studies, such as differences in the potency and specificity of individual drugs and differences in the experimental protocols and animal models. Moreover, it is difficult in principle to evaluate contribution of each prostanoid by the use of COX inhibitors, because each isoform is capable of producing more than one type of prostanoid in a variety of tissues. For example, TXA_2 is produced not only by COX-1 in blood platelets but also by COX-2 in macrophages, which is also believed to produce PGE_2 in atheromatous plaques. The importance of COX-2 in macrophages was suggested by the reduction in atherogenesis found in $LDLR^{-/-}$ mice reconstituted with $COX\text{-}2^{-/-}$ fetal liver cells (15).

In order to conquer these limitations, we have examined the development of atherosclerosis in mice deficient in prostanoid receptors for individual molecules (TXA_2 and PGI_2). TXA_2 and PGI_2 exert their effects through interaction with cell surface receptors specific to each molecule, TP and the PGI receptor (IP), respectively (18). These receptors are encoded by distinct genes and are expressed differentially in the body. With the use of homologous recombination, we have generated mice that lack either TP or IP individually and have subjected the mice to models of various diseases to analyze the roles of TXA_2 and PGI_2 (19–29). In this work, we have cross-bred TP- and IP-deficient ($TP^{-/-}$ and $IP^{-/-}$) mice with $apoE^{-/-}$ mice and have analyzed the roles played by TXA_2 and PGI_2 in atherosclerotic lesion development.

Results

Generation and lipid profile of $apoE^{-/-}TP^{-/-}$ and $apoE^{-/-}IP^{-/-}$ double-KO mice. $TP^{-/-}$ and $IP^{-/-}$ mice that had been backcrossed to the C57BL/6 background 10 times each were bred with $apoE^{-/-}$ mice that had been backcrossed to the C57BL/6 background 5 times. The resultant heterozygous mice, $apoE^{+/-}TP^{+/-}$ or $apoE^{+/-}IP^{+/-}$ mice, were cross-bred with each other, and compound mice deficient in both apoE and TP or both apoE and IP were generated. The genes encoding IP and apoE are both located on chromosome 7, with a genetic interval of approximately 1.5 cM. To generate recombination between the genes encoding IP and apoE, we mated pairs of $apoE^{+/-}IP^{+/-}$ double-heterozygous mice and selected offspring null either for *apoE* or *IP* (about 1% of the offspring) and cross-bred them with each other. Loss of TP or IP was assessed by PCR analysis (Figure 1, A and B) and was confirmed by examination of the platelet response to a TP or IP agonist (data not shown). The TP agonist I-BOP induced aggregation of platelets from $apoE^{-/-}$ mice but not of platelets from $apoE^{-/-}TP^{-/-}$ mice, whereas thrombin-induced aggregation occurred similarly in platelets from $apoE^{-/-}$ and $apoE^{-/-}TP^{-/-}$ mice. In contrast, the IP agonist cicaprost inhibited I-BOP–induced platelet aggregation in $apoE^{-/-}$ mice and this response was lost in $apoE^{-/-}IP^{-/-}$ platelets. The apoE deficiency in these mice was verified by measurement of plasma cholesterol levels and PCR analysis. At 20 weeks of age, $apoE^{-/-}TP^{-/-}$ and $apoE^{-/-}IP^{-/-}$ mice showed elevated levels of both total cholesterol (TC) and total triglyceride (TG) similar to those seen in $apoE^{-/-}$ mice (Table 1). Moreover, VLDL-cholesterol (VLDLC), LDL-cholesterol (LDLC), and HDL-cholesterol (HDLC) in $apoE^{-/-}$, $apoE^{-/-}TP^{-/-}$, and $apoE^{-/-}IP^{-/-}$ mice were almost identical. These findings suggest that loss of either TP or IP did not affect the hypercholesterolemia induced by apoE deficiency. $apoE^{-/-}TP^{-/-}$ and $apoE^{-/-}IP^{-/-}$ mice were fertile and apparently healthy. All animals were maintained on a normal chow diet and gained weight in a similar manner (data not shown).

Atherosclerotic lesion development in $apoE^{-/-}TP^{-/-}$ and $apoE^{-/-}IP^{-/-}$ mice. We used male mice of the three strains ($apoE^{-/-}$, $apoE^{-/-}TP^{-/-}$, and $apoE^{-/-}IP^{-/-}$) and examined atherosclerotic lesion development by analysis of cross-sections of the proximal aorta, en face analysis of the total aorta, and analysis of cross-sections of the innominate artery. The cross-sectional analysis of the proximal aorta was performed in the first 360 μm of the aortas of $apoE^{-/-}$, $apoE^{-/-}TP^{-/-}$, and $apoE^{-/-}IP^{-/-}$ mice at 15, 20, and 30 weeks of age. Typical oil red O staining in each strain of mice at the respective age is shown in Figure 1C. The quantitative analysis revealed significant acceleration and delay of lesion development in $apoE^{-/-}IP^{-/-}$ and $apoE^{-/-}TP^{-/-}$ mice, respectively, compared with that in $apoE^{-/-}$ mice (Figure 1D). At 15 and 20 weeks of age, the lesion areas of $apoE^{-/-}IP^{-/-}$ mice (0.206 ± 0.016 mm² and 0.420 ± 0.017 mm²) were augmented significantly by 131% and 45%, respectively, compared with those of $apoE^{-/-}$ mice (0.089 ± 0.015 mm² and 0.290 ± 0.015 mm²; $P < 0.05$, Tukey's *t* test following one-way ANOVA) (Figure 1D). After 20 weeks, lesion development in $apoE^{-/-}IP^{-/-}$ mice appeared to quickly reach a plateau and did not show a significant difference compared with that in $apoE^{-/-}$ mice at 30 weeks of age. In contrast, $apoE^{-/-}TP^{-/-}$ mice showed significant delay in the lesion development; their lesion areas at 20 and 30 weeks of age (0.087 ± 0.015 mm² and 0.183 ± 0.034 mm²) were significantly suppressed, by 70% and 58%, respectively, compared with those of $apoE^{-/-}$ mice (0.290 ± 0.015 mm² and 0.438 ± 0.025 mm²; $P < 0.01$, Tukey's *t* test following one-way ANOVA) (Figure 1D).

$ApoE^{-/-}IP^{-/-}$ and $apoE^{-/-}TP^{-/-}$ mice showed enhancement and suppression, respectively, of atherogenesis not only locally in the aortic sinus but also globally throughout aorta. En face analysis of aortic preparations of mice at 20 weeks of age revealed significant augmentation and reduction in atherosclerotic area in $apoE^{-/-}IP^{-/-}$ and $apoE^{-/-}TP^{-/-}$ mice, respectively, compared with that of $apoE^{-/-}$ mice (Figure 1E); the average lesion size in $apoE^{-/-}TP^{-/-}$ mice (2.8% ± 0.4%) was reduced 71% compared with that in $apoE^{-/-}$ mice (9.6% ± 0.9%; $P < 0.01$, Tukey's *t* test following one-way ANOVA), while that in $apoE^{-/-}IP^{-/-}$ mice (12.3% ± 1.0%) was augmented 28% compared with that in $apoE^{-/-}$ mice ($P < 0.05$, Tukey's *t* test following one-way ANOVA) (Figure 1F). Atherosclerotic lesions in $apoE^{-/-}$ mice were seen in the lesser curvature of the aortic arch and at the ostium of the brachiocephalic artery as well as in the abdominal aorta. The lesions in $apoE^{-/-}TP^{-/-}$ at this age were limited mostly to the aortic arch region, where the extent was much less. In contrast, atherosclerotic lesions in $apoE^{-/-}IP^{-/-}$ mice were more extensive than in $apoE^{-/-}$ mice in every region examined (Figure 1E).

Although analysis of atherogenesis in $apoE^{-/-}$ mice is carried out mostly in the aorta, atherosclerotic lesions in this strain of mice are not limited to the aorta. We noted the atherosclerotic lesion at the ostium of the brachiocephalic (innominate) artery in our en face analysis of 20-week-old mice described above. Recently, Rosenfeld et al. (30) examined the distribution of atherosclerotic lesions throughout the arterial tree of $apoE^{-/-}$ mice and found a highly advanced, clinically significant lesion in the innominate artery in mice 30–60 weeks of age. We therefore examined atherosclerotic lesion development in the innominate artery by cross-sectional analysis in $apoE^{-/-}$, $apoE^{-/-}TP^{-/-}$, and $apoE^{-/-}IP^{-/-}$ mice 45 weeks of age. As shown in the hematoxylin and eosin staining in Figure 1G, the lesion was found in all three strains of mice but the extent differed significantly. Whereas the plaques protruded into the arterial lumen only partially in $apoE^{-/-}$ and $apoE^{-/-}TP^{-/-}$ mice, those in

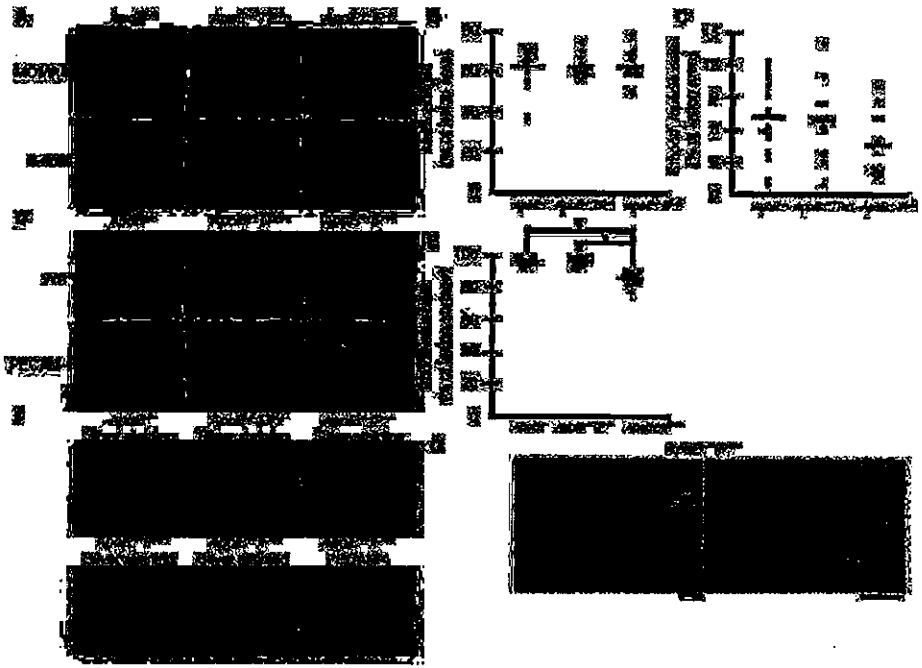

Figure 2
Effects of TP or IP deficiency on the abundance of macrophages and SMCs and EC integrity in aortic arch lesions of apoE-deficient mice at 20 weeks of age. (**A**) Representative immunostaining of macrophages and SMCs in aortic arch lesions of $apoE^{-/-}$ (left panels), $apoE^{-/-}TP^{-/-}$ (middle panels), and $apoE^{-/-}IP^{-/-}$ (right panels) mice. Lesions were stained with specific antibodies for macrophages (MOMA-2; upper) and for SMCs (α-actin; lower). White arrowheads indicate the external elastic lamina. Scale bars: 20 μm. (**B** and **C**) Quantitative analysis of the abundance of macrophages (**B**) and SMCs (**C**) in aortic arch lesions of $apoE^{-/-}$, $apoE^{-/-}TP^{-/-}$, and $apoE^{-/-}IP^{-/-}$ mice. Data are means ± SEM ($n = 10$ each). (**D**) Representative immunostaining of ECs in aortic arch lesions of $apoE^{-/-}$ (left panels), $apoE^{-/-}TP^{-/-}$ (middle panels), and $apoE^{-/-}IP^{-/-}$ (right panels) mice. Cross-sections were stained with specific antibodies for ECs (vWF, upper, and PECAM-1, red, lower) and SMCs (α-actin, green, lower). Black and white arrowheads indicate the site of endothelial disruption. Scale bars: 20 μm. (**E**) Quantitative analysis for endothelial integrity in aortic arch lesions of $apoE^{-/-}$, $apoE^{-/-}TP^{-/-}$, and $apoE^{-/-}IP^{-/-}$ mice by measurement of the vWF-positive signals overlying aortic lesions. Data are means ± SEM ($n = 10$ each). *$P < 0.05$ for bracketed comparisons. (**F**) Representative en face staining of aortic arch lesions of $apoE^{-/-}$, $apoE^{-/-}TP^{-/-}$, and $apoE^{-/-}IP^{-/-}$ mice. En face staining of aortic arch lesions with silver nitrate or anti–PECAM-1 was performed. Scale bars: 10 μm. (**G**) Representative scanning electron micrographs of aortic arches of $apoE^{-/-}IP^{-/-}$ mice. The right panel shows a higher magnification of the boxed area in the left panel. Scale bars: 50 μm.

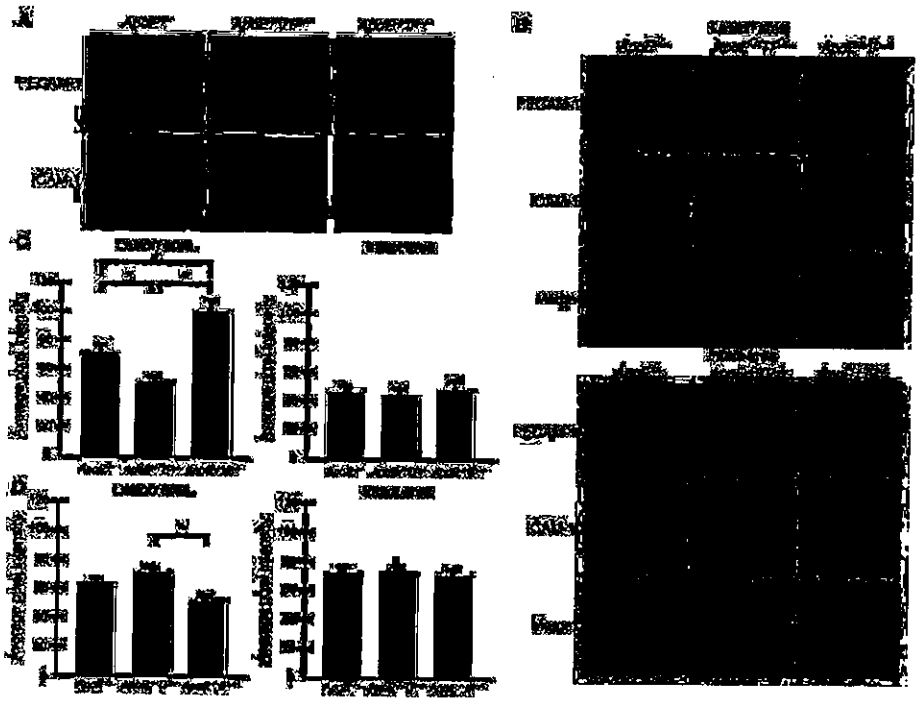

Figure 3
Effects of TP or IP deficiency on ICAM-1 and PECAM-1 expression in the ECs overlying atheromatous lesions of apoE-deficient mice. (A) Representative immunostaining for ICAM-1 and PECAM-1 in cross-sections from *apoE*$^{-/-}$ (left panels), *apoE*$^{-/-}$*TP*$^{-/-}$ (middle panels), and *apoE*$^{-/-}$*IP*$^{-/-}$ (right panels) mice. Mice were sacrificed at 20 weeks of age. Cross-sections were stained with specific antibodies against ICAM-1 (red; lower panels), PECAM-1 (red; upper panels), and smooth muscle α-actin (green). Scale bars: 20 μm. (B) Representative immunostaining of aortic arch lesions and neighboring intact areas for ICAM-1 and PECAM-1 in en face preparations of *apoE*$^{-/-}$ (left panels), *apoE*$^{-/-}$*TP*$^{-/-}$ (middle panels) and *apoE*$^{-/-}$*IP*$^{-/-}$ (right panels) mice. En face preparations were stained with specific antibodies against ICAM-1 (middle panels) and PECAM-1 (upper panels). Mice were sacrificed at 20 weeks of age. Scale bars: 10 μm. Merge, merged images. (C and D) Quantification of ICAM-1 (C) and PECAM-1 (D) expression in ECs overlying aortic arch lesions and neighboring intact areas of *apoE*$^{-/-}$, *apoE*$^{-/-}$*TP*$^{-/-}$, and *apoE*$^{-/-}$*IP*$^{-/-}$ mice. Data are means ± SEM (n = 8 each). $^{*}P < 0.05$ and $^{**}P < 0.01$ for bracketed comparisons.

apoE$^{-/-}$*IP*$^{-/-}$ mice grew extensively to partially occlude the lumen. Quantitative analysis revealed significant acceleration and delay in lesion development, respectively, in *apoE*$^{-/-}$*IP*$^{-/-}$ and *apoE*$^{-/-}$*TP*$^{-/-}$ mice compared with *apoE*$^{-/-}$ mice (Figure 1H).

Impaired EC integrity in atheromatous plaques of apoE$^{-/-}$*IP*$^{-/-}$ *mice.* To investigate whether loss of TP or IP signaling had any effect on the cell composition in atheromatous plaques, we stained macrophages, SMCs, and ECs in the plaques at the aortic arches of 20-week-old mice with antibodies against the respective marker proteins. Quantification of macrophage and SMC abundance in the plaques and of endothelial integrity on the lesion surface was performed on the ten sections taken every 18 μm as described in Methods (Figure 2). Cells staining positive for MOMA-2 were found throughout the plaques in all of *apoE*$^{-/-}$, *apoE*$^{-/-}$*TP*$^{-/-}$, and *apoE*$^{-/-}$*IP*$^{-/-}$ mice at this stage. Quantification revealed that MOMA-2–stained cells occupied about 60% of the total plaque area and there were no significant differences among the three strains (Figure 2, A and B). The fact that the area inside the plaque was stained homogenously with oil red O suggested that these MOMA-2–positive cells represented macrophage-derived foam cells and the space not occupied by macrophages represented mostly lipid cores. SMCs staining positive for α-actin accumulated and formed a layer at the top of the lesion beneath the EC layer (Figure 2A and data not shown). Quantification revealed that they comprised about 7% of the total plaque area in *apoE*$^{-/-}$ and *apoE*$^{-/-}$*TP*$^{-/-}$ mice (Figure 2C). The proportion of SMCs in *apoE*$^{-/-}$*IP*$^{-/-}$ mice tended to be lower than that in the other two strains of mice, but there was no significant difference. This SMC phenotype of *apoE*$^{-/-}$*IP*$^{-/-}$ mice is at odds with the suppression

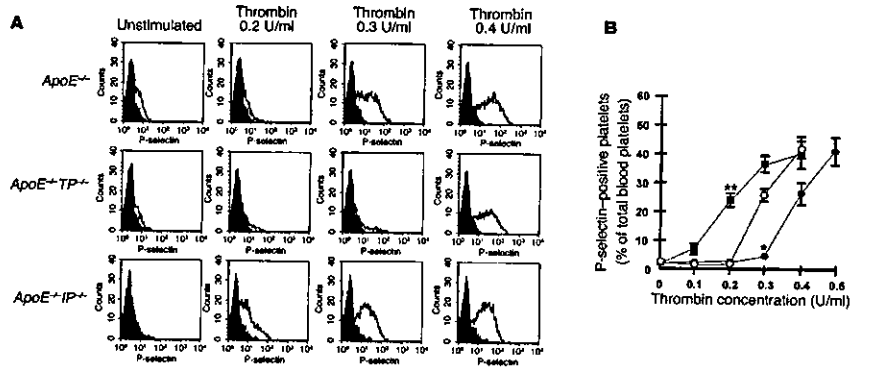

Figure 4
Platelet reactivity for thrombin-induced surface expression of P-selectin. (A) Representative histograms of thrombin-induced P-selectin expression in platelets from *apoE*$^{-/-}$ (upper panels), *apoE*$^{-/-}$*TP*$^{-/-}$ (middle panels), and *apoE*$^{-/-}$*IP*$^{-/-}$ (lower panels) mice. Platelets were either left unstimulated or were stimulated with 0.2, 0.3, or 0.4 U/ml of thrombin. They were then labeled with FITC-conjugated anti–P-selectin and were analyzed by flow cytometry. Filled histograms indicate background signal. (B) Quantification analysis. Concentration-dependent effect of thrombin for P-selectin expression was determined in platelets from *apoE*$^{-/-}$ (open circles), *apoE*$^{-/-}$*TP*$^{-/-}$ (filled circles), and *apoE*$^{-/-}$*IP*$^{-/-}$ (filled squares) mice. Data are means ± SEM (n = 9 each). $^{*}P < 0.05$ and $^{**}P < 0.01$ versus *apoE*$^{-/-}$ mice.

of SMC proliferation by a PGI_2 analog (cicaprost) in vitro (22) as well as the enhanced proliferative response found in IP-deficient mice subjected to chronic hypoxia (23) or catheter-induced carotid vascular injury (31). Impaired SMC proliferation in the absence of IP may suggest that SMC proliferation is under more complex regulation in atherosclerosis or that it may be unique to the apoE-deficient mice. These points should be clarified in future studies.

EC integrity on the plaque surface was then examined by staining of the cross-sections for two endothelial markers: von Willebrand factor (vWF) and platelet endothelial cell adhesion molecule 1 (PECAM-1). As expected, the staining was seen as a linear signal in the EC layer over the plaques. There was occasional loss of staining of these two markers in the plaques of *apoE*$^{-/-}$*IP*$^{-/-}$ mice, especially on the "shoulder" of atherosclerotic lesions (Figure 2D). In contrast, no such irregularity in EC staining on the plaque surface was seen in *apoE*$^{-/-}$ and *apoE*$^{-/-}$*TP*$^{-/-}$ mice. Quantification of vWF staining on the plaque surface revealed a significant reduction in *apoE*$^{-/-}$*IP*$^{-/-}$ mice (85.5% ± 0.7%) compared with *apoE*$^{-/-}$ mice (98.0% ± 0.5%, $P < 0.05$, Tukey's t test following one-way ANOVA) and *apoE*$^{-/-}$*TP*$^{-/-}$ mice (98.5% ± 0.5 %, $P < 0.05$, Tukey's t test following one-way ANOVA) (Figure 2E). Compatible with these findings in the cross-sections, staining of en face preparations with silver nitrate as well as anti-PECAM revealed loss of ECs which was consistently associated with the "shoulder" of a plaque in *apoE*$^{-/-}$*IP*$^{-/-}$ mice (Figure 2F). Such EC loss was rarely seen in *apoE*$^{-/-}$ and *apoE*$^{-/-}$*TP*$^{-/-}$ mice (observations of 5 mice of each strain). Scanning electron microscopy of the aortic arch region revealed again focal endothelial disruption in the "shoulder" of atheromatous plaques of all of three *apoE*$^{-/-}$*IP*$^{-/-}$ mice examined, while none of three *apoE*$^{-/-}$ or *apoE*$^{-/-}$*TP*$^{-/-}$ mice showed such lesions. In some cases, the lesion of endothelial disruption formed a crater in which monocyte/macrophage–like cells accumulated (Figure 2G). These findings suggest that the EC loss had already occurred in vivo and was not an artifact created during sample preparation.

ICAM-1 and PECAM-1 expression on ECs in apoE$^{-/-}$*TP*$^{-/-}$ *and apoE*$^{-/-}$*IP*$^{-/-}$ *mice.* To explore endothelium activation in *apoE*$^{-/-}$*TP*$^{-/-}$ and *apoE*$^{-/-}$*IP*$^{-/-}$ mice, we stained for ICAM-1 and PECAM-1 in ECs overlying the lesions of the three lines of mice. In cross-sections, PECAM-1 expression was found more or less homogenously through the EC monolayer overlying the lesions, while ICAM-1 expression by endothelium was most intense at borders and the "shoulder" of the lesions in all of the three strains of mice (Figure 3A). We then performed quantitative analysis using en face confocal microscopy images (Figure 3B). In the ECs overlying the lesions, *apoE*$^{-/-}$*TP*$^{-/-}$ mice had a significant decrease in ICAM-1 expression (53.9 ± 1.8 versus 73.1 ± 4.1; $P < 0.05$, Tukey's t test following one-way ANOVA; values measured in arbitrary units based on fluorescence intensity per pixel) compared with that of *apoE*$^{-/-}$ mice, whereas ICAM-1 expression in *apoE*$^{-/-}$*IP*$^{-/-}$ mice significantly increased (100.5 ± 7.6; $P < 0.01$, Tukey's t test following one-way ANOVA) (Figure 3C). In contrast, there was no difference in ICAM-1 expression in ECs in intact areas among the three strains of mice, which was low compared with that in the atherosclerotic lesions. As for PECAM-1 expression in the atherosclerotic lesions, expression in *apoE*$^{-/-}$*TP*$^{-/-}$ mice or *apoE*$^{-/-}$*IP*$^{-/-}$ mice tended to increase or decrease, respectively, compared with that in *apoE*$^{-/-}$ mice, and there was a significant difference in expression between *apoE*$^{-/-}$*IP*$^{-/-}$ and *apoE*$^{-/-}$*TP*$^{-/-}$ mice (52.4 ± 3.2 versus 68.3 ± 1.7; $P < 0.05$, Tukey's t test following one-way ANOVA) (Figure 3D). There was also no difference in PECAM-1 expression in the ECs of intact areas among the three strains of mice.

Reactivity of platelets in apoE$^{-/-}$*, apoE*$^{-/-}$*TP*$^{-/-}$*, and apoE*$^{-/-}$*IP*$^{-/-}$ *mice.* Because TXA_2 and PGI_2 are potent activators and suppressors, respectively, of blood platelets, chronic loss of their actions may cause alterations in platelet reactivity to an aggregating agent. Reactivity of blood platelets was therefore compared among *apoE*$^{-/-}$, *apoE*$^{-/-}$*TP*$^{-/-}$, and *apoE*$^{-/-}$*IP*$^{-/-}$ mice by whole-blood flow cytometry (32, 33). Briefly,

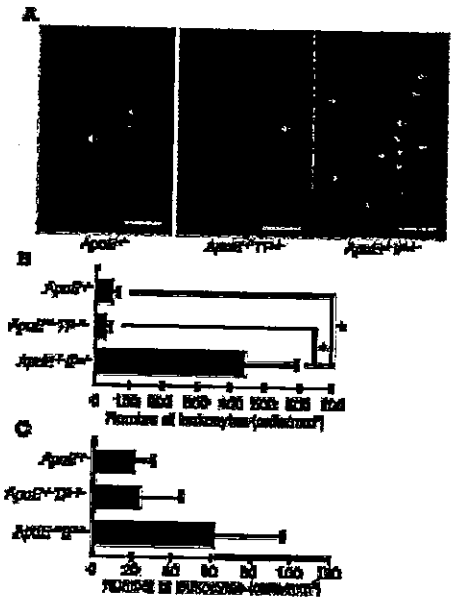

Figure 5
Intravital microscopy for leukocyte rolling and adhesion. (A) Fluorescence images of rolling and adherent leukocytes. Black and white arrows indicate rolling and adherent leukocytes, respectively. Vessel lumens are outlined by broken lines. Scale bars: 0.1 mm. (B) Quantitative analysis of rolling leukocytes. Data are means ± SEM ($n = 5$ each). *$P < 0.05$ versus *apoE*$^{+/+}$ and *apoE*$^{+/+}$*TP*$^{-/-}$ mice. (C) Quantitative analysis for adherent leukocytes as described in B.

diluted blood was activated with various concentrations of thrombin and expression of P-selectin on the platelet surface was evaluated by flow cytometry. Expression of P-selectin was barely detected on unstimulated platelets, but the number of blood platelets showing surface P-selectin expression increased with increasing concentrations of thrombin. P-selectin expression was induced significantly with 0.3 U/ml thrombin and increased with 0.4 U/ml thrombin on the platelets of *apoE*$^{-/-}$ mice (Figure 4, A and B), whereas its expression was only marginally induced at 0.3 U/ml thrombin in the platelets of *apoE*$^{-/-}$*TP*$^{-/-}$ mice (Figure 4, A and B). In contrast, an increase in the P-selectin expression was detected at doses as low as 0.1 U/ml and increased significantly with 0.2 U/ml thrombin in the platelets of *apoE*$^{-/-}$*IP*$^{-/-}$ mice (Figure 4, A and B). These results indicate that the platelets of *apoE*$^{-/-}$*TP*$^{-/-}$ and *apoE*$^{-/-}$*IP*$^{-/-}$ mice have lower and higher sensitivity to thrombin, respectively, than those of *apoE*$^{-/-}$ mice.

Leukocyte adherence in the common carotid arteries of apoE$^{-/-}$*IP*$^{-/-}$ *mice.* Finally, we examined the leukocyte-EC interaction by intravital microscopy. Rhodamine 6G was injected i.v. into *apoE*$^{-/-}$, *apoE*$^{-/-}$*TP*$^{-/-}$, and *apoE*$^{-/-}$*IP*$^{-/-}$ mice to label leukocytes in vivo, and interaction of the leukocytes with the wall of the common carotid artery was examined by intravital microscopy. Leukocytes rolling or adhering were seen as fluorescent dots on the wall of the artery (Figure 5A). Quantitative analysis revealed a significantly greater number of leukocytes rolling on the walls of arteries in *apoE*$^{-/-}$*IP*$^{-/-}$ mice than in either *apoE*$^{-/-}$ or *apoE*$^{-/-}$*TP*$^{-/-}$ mice (Figure 5B). Additionally, adhesion of leukocytes also tended to be higher in *apoE*$^{-/-}$*IP*$^{-/-}$ mice (Figure 5C). Although rhodamine 6G also labeled platelets, we did not see thrombus formation or detachment in any strain of mice during our observation period.

Discussion

TXA_2 and PGI_2 are two major prostanoids in the cardiovascular system, being abundantly produced by blood platelets and vascular endothelium, respectively. Previous studies found that TXA_2 and PGI_2 biosynthesis is increased in patients with atherosclerosis (2, 3). In this work, we generated compound mice, *apoE*$^{-/-}$*TP*$^{-/-}$ and *apoE*$^{-/-}$*IP*$^{-/-}$, and examined the roles of TXA_2 and PGI_2 in the initiation and progression of atherosclerosis. *ApoE*$^{-/-}$ mice develop a spectrum of atherosclerotic lesions similar to that of humans (34). They also show elevated production of TXA_2 and PGI_2, as seen in humans (35). Thus, the *apoE*$^{-/-}$ mouse is a suitable animal model for evaluation of the roles of TXA_2 and PGI_2 in atherosclerosis. Previously, the involvement of these prostanoids in atherosclerosis was examined by the use of various COX inhibitors in this and similar animal models. However, the results obtained by those studies were variable (7, 8, 14–17). In addition, a study using a TP antagonist in *apoE*$^{-/-}$ mice showed only a marginal reduction in atherogenesis (8). In contrast to those findings in the previous studies, our study here using genetically engineered mice has demonstrated significant suppression and significant enhancement of atherosclerosis in *apoE*$^{-/-}$*TP*$^{-/-}$ and *apoE*$^{-/-}$*IP*$^{-/-}$ mice, respectively, suggesting strongly proatherogenic and antiatherogenic actions of TXA_2 and PGI_2, respectively. TP deficiency suppressed the extent of atherosclerosis at both 20 and 30 weeks of age. Suppression of atherosclerosis by TP deficiency is much more robust (70% at 20 weeks of age and 58% at 30 weeks of age) than that found after treatment with the TP antagonist S-18886 (about 20%) (8). We have also examined the effects of TP or IP deficiency on the development of vascular lesions in the innominate arteries of 45-week-old *apoE*$^{-/-}$ mice. Rosenfeld et al. (30) previously noted more-advanced vascular lesions in the innominate arteries in *apoE*$^{-/-}$ mice. In this study we have not only confirmed their findings in *apoE*$^{-/-}$ mice but also found that this lesion was far more advanced in *apoE*$^{-/-}$*IP*$^{-/-}$ mice, whereas the disease progression appeared to be retarded in *apoE*$^{-/-}$*TP*$^{-/-}$ mice.

It is noteworthy that atherogenesis was significantly accelerated and reached a plateau early in *apoE*$^{-/-}$*IP*$^{-/-}$ mice compared with *apoE*$^{-/-}$ mice. These results indicate that signaling from PGI_2 to IP is important in preventing the initiation of atherosclerosis. Impaired PGI_2 function, moreover, appeared to affect the progression and nature of atherosclerotic plaques. Our analysis detected frequent loss of ECs in the plaques of *apoE*$^{-/-}$*IP*$^{-/-}$ mice. In addition to ECs, we also found that the abundance of SMCs tended to be lower in the plaques of *apoE*$^{-/-}$*IP*$^{-/-}$ mice (Figure 2). Lesions with impaired EC integrity and weaker fibrous caps are suggested to be prone to rupture (36). Recently, Cipollone and colleagues found that COX-2 and membrane-bound PGE synthetase are upregulated in macrophages in atheromatous plaques of humans and induce expression of matrix metalloproteinase-9 and proposed that this pathway leads to plaque instability (37, 38). It is interesting in this context that PGI_2 can suppress expression of this matrix metalloproteinase isoform in vitro and in vivo (39, 40). Lesion rupture, when it occurs in vivo, then precipitates thrombosis, which is further accelerated in the absence of IP. Disruption of IP is known to increase the risk of thrombosis (20). Thus, PGI_2 appears to exert important inhibitory actions on the initiation and progression of atherosclerosis, and the reduction in PGI_2 in the presence of normal TXA_2 formation is likely to lead an increased risk of atherosclerosis and thrombosis. Currently, an important question concerning COX-2 inhibitors is whether the selective reduction in PGI_2 increases the risk of atherosclerosis. Our findings support that conclusion. However, our findings cannot be directly extrapolated to the clinical outcome of patients treated with COX-2 inhibitors. Although the majority of PGI_2 under basal conditions is derived from COX-2 catalysis, both COX-1 and COX-2 contribute to the increase in PGI_2 in patients with atherosclerosis as well as in *apoE*$^{-/-}$ mice (3, 17), and selective inhibition of COX-2 usually results in only partial inhibition of PGI_2 production (15–17). In addition, TXA_2 can be derived also from COX-2 in atherosclerotic plaques. COX-2 is expressed by monocytes/macrophages in mouse atherosclerotic lesions (15). Macrophages contain TX synthase and release large amounts of TXA_2 when transformed into foam cells with modified LDL (41).

What, then, are the underlying mechanisms of the actions of TXA_2 and PGI_2 in atherogenesis? Activation and inhibition of blood platelets by TXA_2 and PGI_2, respectively, may certainly be one of the mechanisms. Activated platelets were found in the circulating blood of patients with atherosclerosis (42–44) and hypercholesterolemia (45, 46). We have examined this issue by using whole-blood flow cytometry for thrombin-induced P-selectin expression in platelets (32). This method has been used frequently to evaluate platelet reactivity in patients with various cardiovascular disorders (33). Our analysis has revealed that platelets of *apoE*$^{-/-}$*TP*$^{-/-}$ and *apoE*$^{-/-}$*IP*$^{-/-}$ mice have lower and higher reactivity, respectively, than those of *apoE*$^{-/-}$ mice, which is consistent with the atherosclerotic phenotypes observed in the three strains of mice.

Here, we have further examined effects of TP or IP disruption on expression of adhesion molecules on ECs. Adhesion molecules on ECs play important roles in the migration of monocytes/macrophages through the EC monolayer and the initiation of atheromatous plaques. Indeed, ICAM-1 is strongly expressed in atherosclerotic plaques of humans (47) and the level of soluble ICAM-1 correlates with the severity of atherosclerosis (48). In *apoE*$^{-/-}$ mice, ICAM-1 expression is high in atherosclerosis-prone sites of the aorta, and deficiency in ICAM-1 in apoE-deficient mice significantly reduces atherosclerotic lesions (49). We have found that ICAM-1 expression on ECs overlying the plaques of *apoE*$^{-/-}$*TP*$^{-/-}$ mice is significantly lower, while that of *apoE*$^{-/-}$*IP*$^{-/-}$ mice is significantly higher, than ICAM-1 expression in *apoE*$^{-/-}$ mice (Figure 3). The changes in the ICAM-1 expression in the presence of TP or IP deficiency are consistent with the reported in vitro actions of TXA_2 and PGI_2. ICAM-1 expression is induced by proinflammatory cytokines from activated macrophages such as TNF-α or IL-1β (50). Signaling from PGI_2 to IP is known to inhibit TNF-α production by activated macrophages (21) and to reduce IL-1–induced ICAM-1 expression on ECs (51). In contrast, stimulation of TP induces ICAM-1 expression in cultured ECs in vitro (52, 53), suggesting that TXA_2 formed in situ in atheromatous plaques acts on ECs to induce ICAM-1 expression to amplify atherogenesis. Interestingly, TXA_2 and PGI_2 appear to have effects opposite to those of ICAM-1 on the expression of PECAM-1 on the plaque ECs, which was up- and downregulated in *apoE*$^{-/-}$*TP*$^{-/-}$ and *apoE*$^{-/-}$*IP*$^{-/-}$ mice, respectively. PECAM-1 was first described as an adhesion molecule essential in the transmigration of leukocytes through endothelial monolayer (54). However, recent analyses of *PECAM-1*$^{-/-}$ mice in various models showed that PECAM-1 deficiency did not block but instead enhanced leukocyte accumulation at inflammation sites (55–57). Given its intracellular domain, PECAM-1 is now suggested to be an inhibitory signaling molecule (58). Intriguingly, regulation of PECAM-1 expression is opposite to that of ICAM-1. For example, a previous report showed that the expression of PECAM-1 and ICAM-1 on cultured human umbilical vein ECs was down- and upregulared, respectively, after activation with TNF-α plus IFN-γ (59). Such opposite modes of expression may explain the changes in the patterns of ICAM-1 and PECAM-1 expression found in the atherosclerosis phenotypes of *apoE*$^{-/-}$*TP*$^{-/-}$ and *apoE*$^{-/-}$*IP*$^{-/-}$ mice.

The above findings on the reactivity of platelets and the expression of adhesion molecules in ECs in *apoE*$^{-/-}$, *apoE*$^{-/-}$*TP*$^{-/-}$, and *apoE*$^{-/-}$*IP*$^{-/-}$ mice suggest that TP or IP deficiency can affect the interaction of ECs with platelets and leukocytes. We examined this issue by intravital microscopy. Although we did not detect significant platelet adhesion to the blood vessels of any of the three lines of mice under basal conditions, we found significant leukocyte adherence to the wall of the common carotid artery in *apoE*$^{-/-}$*IP*$^{-/-}$ mice. This may be relevant to the higher platelet reactivity and enhanced ICAM-1 expression in this line of animals. Platelet P-selectin is suggested to play an important role in mediating the leukocyte-EC interaction (60). It may be also relevant to the EC disruption observed in *apoE*$^{-/-}$*IP*$^{-/-}$ mice.

In conclusion, using the IP-deficient and TP-deficient mice, we were able to evaluate separately the contributions of PGI_2 and TXA_2 to the development of atherosclerosis. The information presented here will aid in the interpretation of clinical findings and the evaluation of risk in atherosclerotic patients treated with various drugs modulating the arachidonate cascade. Our findings also indicate that the administration of PGI mimetics and TP antagonists may be useful in the prevention of atherosclerosis. This line of genetic approach may also help to identify the contributions of PGs other than PGI_2 and TXA_2 to atherosclerosis.

Methods

Generation of apoE$^{-/-}$*TP*$^{-/-}$ *and apoE*$^{-/-}$*IP*$^{-/-}$ *double-KO mice.* *ApoE*$^{-/-}$ mice (129Ola × C57BL/6 mixed background) were a generous gift from Edward M. Rubin (University of California at Berkeley, Berkeley, California, USA) (4). Mice lacking TP or IP individually were generated as described (19, 20). *ApoE*$^{-/-}$, *TP*$^{-/-}$, and *IP*$^{-/-}$ mice were backcrossed 5, 10, and 10 times, respectively, to C57BL/6CrSlc mice (Japan SLC). *TP*$^{-/-}$ and *IP*$^{-/-}$ mice were then cross-bred with *apoE*$^{-/-}$ mice. Functional disruption of the gene encoding apoE was confirmed by markedly elevated plasma cholesterol levels. Genotype analyses of *apoE*$^{-/-}$, *TP*$^{-/-}$, and *IP*$^{-/-}$ mice were performed by PCR using genomic DNA isolated from tail snip samples as a template. PCR analysis was performed for apoE alleles with the sense primers exon2 (5′-GTGCTGTTGGTCACATTGCTGACA-3′) and Neo1 (5′-ATGGGATCGGCCATTGAACA-3′) for WT and mutant alleles, respectively, and the antisense primer exon3 (5′-TCAGTTCTTGTGTGACTTGGGAGC-3′); for TP alleles with the sense primers ML139 (5′-ACTTTGTTGCAGACACCACCTGTC-3′) and Neo2 (5′-TGATATTGCTGAAGAGCTTGGCGGCGA-3′) for WT and mutant alleles, respectively, and the antisense primer ML136 (5′-AAGCTTGGGTTTCAGGGACCT-3′); and for IP alleles with the sense primer CY37 (5′-GTATCTTTCAGTACCTGAGGACTG-3′) and

the antisense primers CY41 (5′-GAGCAGAAAAATTCCCAGAGGCTT-3′) and Neo17 (5′-TGACCGCTTCCTCGTGCTTTAC-3′) for WT and mutant alleles, respectively (Figure 1A). Reaction mixtures contained 10 mM Tris-HCl, pH 8.3, 50 mM KCl, 1.5 mM $MgCl_2$, 0.1% Triton X-100, 10% DMSO, 0.25 mM dNTPs, 20 pmol of each primer, and 1 U of Taq DNA polymerase (Toyobo) in a total volume of 20 μl. After a denaturation step at 94°C for 3 minutes, 35 cycles of the amplification step (94°C for 60 seconds, 58°C for 60 seconds, and 72°C for 80 seconds) were carried out, followed by a final elongation step of 3 minutes at 72°C. For apoE alleles, primers exon2 and exon3 amplify a 0.7-kb WT allele fragment, and primers Neo1 and exon3 amplify a 0.4-kb mutant allele fragment. For TP alleles, primers ML139 and ML136 amplify a 0.9-kb WT allele fragment, and primers Neo2 and ML136 amplify a 1.1-kb mutant allele fragment (Figure 1A). For IP alleles, primers CY37 and CY41 amplify a 1.3-kb WT allele fragment, and primers CY37 and Neo17 amplify a 0.9-kb mutant allele fragment (Figure 1A). Mice were kept on a 12-hour light/dark cycle and were fed a normal chow diet (F2; Funabashi Farm). Food and water were available ad libitum. All experiments were performed in male mice. All experimental procedures were approved by the Committee on Animal Research of Kyoto University Faculty of Medicine.

Preparation of mouse platelets and platelet aggregation assay. Platelet aggregation was examined as described previously (61). Blood (1.0 ml) was drawn by cardiac puncture of ether-anesthetized mice with a syringe containing 50 μl of 3.8% trisodium citrate. Blood pooled from 3–4 animals was diluted with an equal volume of modified Tyrode-HEPES buffer, pH 7.4 (20 mM HEPES, 140 mM NaCl, 5 mM $MgCl_2$, and 5 mM KCl). Platelet-rich plasma (PRP) was prepared by centrifugation at 160 *g* for 5 minutes at room temperature. Platelet-poor plasma was obtained by further centrifugation of the blood after PRP was removed at 1,500 *g* for 10 minutes at room temperature. The number of platelets in the PRP was adjusted to 3×10^5 platelets/μl. Platelet aggregation was measured with an aggregometer (NBS Hema Tracer 601; Tokyo Koden). I-BOP, a TP agonist, was used to activate platelets, and cicaprost, an IP agonist, was used to inhibit platelet aggregation.

Lipid and lipoprotein analyses. Blood (1.0 ml) was drawn by cardiac puncture of ether-anesthetized mice into a tube containing EDTA (final concentration, 5 mM). Plasma was isolated by centrifugation at 1,500 *g* for 10 minutes and was maintained at 4°C. Plasma cholesterol and triglyceride were measured using Toyobo enzymatic assay kits (Toyobo). For quantification of the cholesterol content of each lipoprotein, lipoproteins were separated at buoyant densities of 1.019 g/ml and 1.063 g/ml by ultracentrifugation. VLDLC is the difference between TC and cholesterol with a density greater than 1.019 g/ml; HDLC is cholesterol with a density of more than 1.063 g/ml cholesterol; LDLC is the difference between TC and the sum of VLDLC and HDLC.

Quantification of atherosclerosis. Atherosclerotic lesions were quantified by en face analysis of the whole aorta and by cross-sectional analysis of the proximal aorta and the innominate artery. For en face preparations of the aorta, a cannula was inserted into the left ventricle and the aortic tree was fixed by perfusion for 10 min with ice-cold PBS containing 4% paraformaldehyde (PFA), 5% sucrose, 20 μM butylated hydroxytoluene, and 2 μM EDTA, as described previously (62, 63). The aorta was opened longitudinally, from the heart to the iliac arteries, while still attached to the heart and major branching arteries in the body. The primary incision followed the ventral side of the aorta and the inner curvature of the arch. To obtain a flat preparation for imaging, a second incision was made along the outer curvature of the arch. The aorta (from the heart to the iliac bifurcation) was then removed and was "pinned out" on a black wax surface in a dissecting pan using stainless steel pins 0.2 mm in diameter. After overnight fixation with the PFA solution described above and a 12-hour rinse in PBS, the aortas were briefly rinsed in 70% ethanol; immersed for 6 minutes in a filtered solution containing 0.5% Sudan IV, 35% ethanol, and 50% acetone; and destained for 5 minutes in 80% ethanol. The Sudan IV–stained aortas were photographed and were used for quantification of atherosclerotic lesions.

For cross-sectional analysis of the aorta, hearts were isolated from mice sacrificed by cervical dislocation, were washed in PBS, and were embedded in OCT compound. The OCT-embedded hearts were sectioned with a cryostat, and 6-μm sections in the proximal aorta were obtained sequentially beginning at the aortic valve. Sections were transferred onto a Superfrost slide (Matsunami) and were stained with oil red O followed by counterstaining with hematoxylin (4). Ten sections obtained every 36 μm from the aortic sinus were used for quantification of lesion areas with Image Pro Plus software (Media Cybernetics). The average lesion area of the ten sections from each heart was taken as a value to represent that animal, and the means of the average lesion areas from each group were compared as described previously (64, 65).

Atherosclerotic lesions in the innominate artery were quantified by cross-sectional analysis. Innominate arteries were isolated from 45-week-old male mice sacrificed by cervical dislocation, were washed in PBS, and were embedded in OCT compound. OCT-embedded innominate arteries were sectioned with a cryostat and 8-μm sections were obtained sequentially. Sections were transferred onto a Superfrost slide and were stained with hematoxylin and eosin. Ten sections obtained every 80 μm were used for quantification of lesion areas with Image Pro Plus software. The average lesion area of the 10 sections from each innominate artery was taken as a value to represent that animal and the means of the average lesion areas from 10 mice were compared.

Immunohistochemistry. For cross-sectional analyses, the aortic tree was perfused with ice-cold PBS containing 5 mM EDTA via a cannula inserted into the left ventricle for 10 minutes. The aortic arch was isolated, embedded in OCT compound, and sectioned at a thickness of 6 μm with a cryostat. Sections containing atherosclerotic plaques were identified by microscopy. These sections were then fixed in 4% PFA at 4°C for 10 minutes, were immersed in PBS for 5 minutes for rehydration of the tissues, and were blocked overnight at 4°C with 2% skim milk (BD) in PBS. For evaluation of the abundance of macrophages and SMCs and the expression of ICAM-1 (CD54) and PECAM-1 (CD31) in the lesions, sections were incubated overnight at 4°C with a 1:200 dilution of rat MOMA-2 mAb against mouse macrophages (Accurate Chemical and Scientific Co.); a 1:200 dilution of mouse 1A4 mAb against human α-smooth muscle actin, labeled with FITC (Dako); a 1:200 dilution of armenian hamster mAb against mouse ICAM-1, labeled with Texas Red (BD); and a 1:200 dilution of rat mAb against mouse PECAM-1, labeled with FITC or Texas Red (BD). Sections incubated with MOMA-2 antibody were then washed and incubated with a 1:400 dilution of goat anti-rat IgG, labeled with Texas Red (BD). For vWF staining, endogenous peroxidase activity was blocked by incubation of sections at 4°C for 30 minutes with 0.3% (volume/volume) H_2O_2 in PBS. The sections were then incubated overnight at 4°C with a 1:200 dilution of mouse mAb against human vWF, labeled with HRP (Sigma-Aldrich). After a thorough washing, staining was developed with diaminobenzidine followed by counterstaining with hematoxylin. Ten sections obtained every 18 μm from aortic arch were used for quantification of the macrophages and SMCs and EC density of the lesions with Image-Pro Plus software. The macrophages and SMCs were quantified by measurement of the area that stained positive for the respective markers, as described previously (7). EC density was determined by the ratio of the vWF-positive luminal surface length to the total luminal surface length of each cross-sectional plaque. The average of the 10 sections was taken to represent 1 animal, and the means of the averages from each group were compared.

For the en face analysis, the aortic tree was first washed by perfusion with ice-cold PBS containing 5 mM EDTA and then was fixed by perfusion with ice-cold PBS containing 4% PFA via a cannula inserted into the left ventricle, each perfusion for 10 minutes. The aortic arch was isolated and opened longitudinally. En face preparations were blocked overnight at 4°C with 2% skim milk in PBS and were incubated overnight at 4°C with a 1:500 dilution of rat mAb against mouse PECAM-1, labeled with FITC, and armenian hamster mAb against mouse ICAM-1, labeled with Texas Red. Because activation of ECs occurs on the "shoulder" of plaques (66), five images (1,024 × 1,024 pixels/image) were obtained randomly from the EC monolayer on the "shoulder" of plaques with a Bio-Rad MRC-1024 confocal microscope. The average pixel intensity of the five images was taken as a value to represent that animal, and the means of the average pixel intensity from each group were compared as described previously (60).

Silver nitrate staining of en face endothelial cells. The aortic tree was washed, stained, and fixed as described previously (67, 68) by successive perfusion in the following solutions: 10 ml of 5% glucose; 4 ml of 0.25% silver nitrate; 2 ml of 5% glucose; 8 ml of 3% cobalt bromide and 1% ammonium bromide; 2 ml of 5% glucose; 4 ml of 4% PFA; 10 ml of distilled water; 2 ml of hematoxylin; and 10 ml of distilled water. The aortic arch was isolated, opened longitudinally, and mounted with the endothelium upward on a Superfrost slide.

Scanning electron microscopy. The aortic trees of 20-week-old male mice were washed at 37°C for 10 minutes with PBS and were fixed at room temperature for 10 minutes with PBS containing 1% glutaraldehyde by perfusion, as described previously (69). The aortic tree was then excised, opened longitudinally, additionally fixed by immersion in PBS containing 1% glutaraldehyde at room temperature for 24 hours, dehydrated in ethanol, and processed by critical point drying with CO_2. The aortic tree specimens were then oriented with the lumens exposed, mounted with carbon paint, and coated with gold for scanning electron microscopy (T-330; Nippon Denshi).

Flow cytometry for platelet reactivity. Platelet reactivity was examined by whole-blood flow cytometry (32, 33). Blood (1.0 ml) was drawn by cardiac puncture of ether-anesthetized mice with a syringe containing 50 μl of 3.8% trisodium citrate. Within 10 minutes of being drawn, the blood was diluted 1:4 in modified Tyrode-HEPES buffer, pH 7.4, and the diluted blood was activated at 37°C for 10 minutes with 0.1–0.5 U/ml thrombin, incubated at room temperature for 30 minutes with a 1:100 dilution of rat mAb against mouse P-selectin, labeled with FITC, and fixed at 4°C for 2 hours with ice-cold PBS containing 1% PFA. Samples were then analyzed using a FACSVantage flow cytometer (BD).

Intravital microscopy. Leukocyte-EC interaction was examined by intravital microscopy using rhodamine 6G that stained in vivo leukocytes, as described previously (29, 60, 69). Five male mice 25–30 weeks of age were used for each strain. Rhodamine 6G was injected i.v., and the numbers of leukocytes rolling on and adhering to the wall of the common carotid artery were examined "off-line" during video playback analysis. A leukocyte was defined as rolling if it migrated along the vessel wall at a rate less than 200 μm/s and as adhering if it remained stationary for more than 20 seconds. We counted the number of leukocyte rolling and adhering in the artery per microscope field (×100) and expressed the results as the number of leukocytes observed per mm^2 area per minute.

Statistical analysis. Data are presented as means ± SEM. Comparison of two groups was analyzed by Student's *t* test. For comparison of more than two groups with comparable variances, one-way ANOVA was performed, followed by Tukey's *t* test to evaluate pair-wise group differences. An associated probability (*P* value) of less than 0.05 was considered significant. Analyses were performed with the use of GraphPad Software Prism 3.0.

Acknowledgments

We are grateful to H. Wise for helpful discussions; K. Deguchi, T. Fujiwara, and N. Kitagawa for animal care and breeding; and T. Arai, H. Nose, and Y. Kitagawa for secretarial assistance. This work was supported in part by Grants-in-Aid for Scientific Research from the Ministry of Education, Science, Sports and Culture of Japan and by grants from the Organization for Pharmaceutical Safety and Research and the Kowa Life Science Foundation.

Received for publication March 1, 2004, and accepted in revised form July 27, 2004.

Address correspondence to: Shuh Narumiya, Department of Pharmacology, Kyoto University Faculty of Medicine, Yoshida, Sakyo-ku, Kyoto 606-8501, Japan. Phone: +81-75-753-4392; Fax: +81-75-753-4693; E-mail: snaru@mfour.med.kyoto-u.ac.jp.

1. Ross, R. 1999. Atherosclerosis is an inflammatory disease. *Am. Heart J.* 138:S419–S420.
2. FitzGerald, G.A., Smith, B., Pedersen, A.K., and Brash, A.R. 1984. Increased prostacyclin biosynthesis in patients with severe atherosclerosis and platelet activation. *N. Engl. J. Med.* 310:1065–1068.
3. Belton, O., Byrne, D., Kearney, D., Leahy, A., and Fitzgerald, D.J. 2000. Cyclooxygenase-1 and -2-dependent prostacyclin formation in patients with atherosclerosis. *Circulation.* 102:840–845.
4. Plump, A.S., et al. 1992. Severe hypercholesterolemia and atherosclerosis in apolipoprotein E-deficient mice created by homologous recombination in ES cells. *Cell.* 71:343–353.
5. Zhang, S.H., Reddick, R.L., Piedrahita, J.A., and Maeda, N. 1992. Spontaneous hypercholesterolemia and arterial lesions in mice lacking apolipoprotein E. *Science.* 258:468–471.
6. Ishibashi, S., et al. 1993. Hypercholesterolemia in low density lipoprotein receptor knockout mice and its reversal by adenovirus-mediated gene delivery. *J. Clin. Invest.* 92:883–893.
7. Cyrus, T., et al. 2002. Effect of low-dose aspirin on vascular inflammation, plaque stability, and atherogenesis in low-density lipoprotein receptor-deficient mice. *Circulation.* 106:1282–1287.
8. Cayatte, A.J., et al. 2000. The thromboxane receptor antagonist S18886 but not aspirin inhibits atherogenesis in apo E-deficient mice: evidence that eicosanoids other than thromboxane contribute to atherosclerosis. *Arterioscler. Thromb. Vasc. Biol.* 20:1724–1728.
9. Vane, J.R., Bakhle, Y.S., and Botting, R.M. 1998. Cyclooxygenases 1 and 2. *Ann. Rev. Pharmacol. Toxicol.* 38:97–120.
10. McAdam, B.F., et al. 1999. Systemic biosynthesis of prostacyclin by cyclooxygenase (COX)-2: the human pharmacology of a selective inhibitor of COX-2. *Proc. Natl. Acad. Sci. U. S. A.* 96:272–277.
11. Topper, J.N., Cai, J., Falb, D., and Gimbrone, M.A., Jr. 1996. Identification of vascular endothelial genes differentially responsive to fluid mechanical stimuli: cyclooxygenase-2, manganese superoxide dismutase, and endothelial cell nitric oxide synthase are selectively up-regulated by steady laminar shear stress. *Proc. Natl. Acad. Sci. U. S. A.* 93:10417–10422.
12. Foeldvari, I. 2002. A selective COX-2 inhibitor, meloxicam, as a treatment option in patients with juvenile idiopathic arthritis and gastrointestinal side effects from naproxen [letter]. *Clin. Exp. Rheumatol.* 20:874.
13. Mukherjee, D., Nissen, S.E., and Topol, E.J. 2001. Risk of cardiovascular events associated with selective COX-2 inhibitors. *JAMA.* 286:954–959.
14. Rott, D., et al. 2003. Effects of MF-tricyclic, a selective cyclooxygenase-2 inhibitor, on atherosclerosis progression and susceptibility to cytomegalovirus replication in apolipoprotein-E knockout mice. *J. Am. Coll. Cardiol.* 41:1812–1819.
15. Burleigh, M.E., et al. 2002. Cyclooxygenase-2 promotes early atherosclerotic lesion formation in LDL receptor-deficient mice. *Circulation.* 105:1816–1823.
16. Pratico, D., Tillmann, C., Zhang, Z.B., Li, H., and FitzGerald, G.A. 2001. Acceleration of atherogenesis by COX-1-dependent prostanoid formation in low density lipoprotein receptor knockout mice. *Proc. Natl. Acad. Sci. U. S. A.* 98:3358–3363.
17. Belton, O.A., Duffy, A., Toomey, S., and Fitzgerald, D.J. 2003. Cyclooxygenase isoforms and platelet vessel wall interactions in the apolipoprotein E knockout mouse model of atherosclerosis. *Circulation.* 108:3017–3023.
18. Narumiya, S., Sugimoto, Y., and Ushikubi, F. 1999. Prostanoid receptors: structures, properties, and functions. *Physiol. Rev.* 79:1193–1226.
19. Kabashima, K., et al. 2003. Thromboxane A_2 modulates interaction of dendritic cells and T cells and regulates acquired immunity. *Nat. Immunol.* 4:694–701.
20. Murata, T., et al. 1997. Altered pain perception and inflammatory response in mice lacking